NUREG/CR-6453
ORNL/TM-13204

# H. B. Robinson-2 Pressure Vessel Benchmark


Prepared by
I. Remec, F. B. K. Kam

Oak Ridge National Laboratory


Prepared for
U.S. Nuclear Regulatory Commission

DF02 0/.

## AVAILABILITY NOTICE

Availability of Reference Materials Cited in NRC Publications

Most documents cited in NRC publications will be available from one of the following sources:

1. The NRC Public Document Room, 2120 L Street, NW., Lower Level, Washington, DC 20555-0001

2. The Superintendent of Documents, U.S. Government Printing Office, P. O. Box 37082, Washington, DC 20402-9328

3. The National Technical Information Service, Springfield, VA 22161-0002

Although the listing that follows represents the majority of documents cited in NRC publications, it is not intended to be exhaustive.

Referenced documents available for inspection and copying for a fee from the NRC Public Document Room include NRC correspondence and internal NRC memoranda; NRC bulletins, circulars, information notices, inspection and investigation notices; licensee event reports; vendor reports and correspondence; Commission papers; and applicant and licensee documents and correspondence.

The following documents in the NUREG series are available for purchase from the Government Printing Office: formal NRC staff and contractor reports, NRC-sponsored conference proceedings, international agreement reports, grantee reports, and NRC booklets and brochures. Also available are regulatory guides, NRC regulations in the *Code of Federal Regulations*, and *Nuclear Regulatory Commission Issuances*.

Documents available from the National Technical Information Service include NUREG-series reports and technical reports prepared by other Federal agencies and reports prepared by the Atomic Energy Commission, forerunner agency to the Nuclear Regulatory Commission.

Documents available from public and special technical libraries include all open literature items, such as books, journal articles, and transactions. *Federal Register* notices, Federal and State legislation, and congressional reports can usually be obtained from these libraries.

Documents such as theses, dissertations, foreign reports and translations, and non-NRC conference proceedings are available for purchase from the organization sponsoring the publication cited.

Single copies of NRC draft reports are available free, to the extent of supply, upon written request to the Office of Administration, Distribution and Mail Services Section, U.S. Nuclear Regulatory Commission, Washington, DC 20555-0001.

Copies of industry codes and standards used in a substantive manner in the NRC regulatory process are maintained at the NRC Library, Two White Flint North, 11545 Rockville Pike, Rockville, MD 20852-2738, for use by the public. Codes and standards are usually copyrighted and may be purchased from the originating organization or, if they are American National Standards, from the American National Standards Institute, 1430 Broadway, New York, NY 10018-3308.

NUREG/CR-6453
ORNL/TM-13204

# H. B. Robinson-2 Pressure Vessel Benchmark

Manuscript Completed: October 1997
Date Published: February 1998

Prepared by
I. Remec, F. B. K. Kam

Oak Ridge National Laboratory
Managed by Lockheed Martin Energy Research Corp.

Oak Ridge National Laboratory
Oak Ridge, TN 37831-6363

C. J. Fairbanks, NRC Project Manager

**Prepared for**
**Division of Engineering Technology**
**Office of Nuclear Regulatory Research**
**U.S. Nuclear Regulatory Commission**
**Washington, DC 20555-0001**
**NRC Job Code W6164**

## ABSTRACT

The H. B. Robinson Unit 2 Pressure Vessel Benchmark (HBR-2 benchmark) is described and analyzed in this report. Analysis of the HBR-2 benchmark can be used as partial fulfillment of the requirements for the qualification of the methodology for calculating neutron fluence in pressure vessels, as required by the U.S. Nuclear Regulatory Commission Regulatory Guide DG-1053, *Calculational and Dosimetry Methods for Determining Pressure Vessel Neutron Fluence*.

Section 1 of this report describes the HBR-2 benchmark and provides all the dimensions, material compositions, and neutron source data necessary for the analysis. The measured quantities, to be compared with the calculated values, are the specific activities at the end of fuel cycle 9. The characteristic feature of the HBR-2 benchmark is that it provides measurements on both sides of the pressure vessel: in the surveillance capsule attached to the thermal shield and in the reactor cavity.

In Section 2, the analysis of the HBR-2 benchmark is described. Calculations with the computer code DORT, based on the discrete-ordinates method, were performed with three multigroup libraries based on ENDF/B-VI: BUGLE-93, SAILOR-95 and BUGLE-96. The average ratio of the calculated-to-measured specific activities (C/M) for the six dosimeters in the surveillance capsule was 0.90 ± 0.04 for all three libraries. The average C/Ms for the cavity dosimeters (without neptunium dosimeter) were 0.89 ± 0.10, 0.91 ± 0.10, and 0.90 ± 0.09 for the BUGLE-93, SAILOR-95 and BUGLE-96 libraries, respectively.

It is expected that the agreement of the calculations with the measurements, similar to the agreement obtained in this research, should typically be observed when the discrete-ordinates method and ENDF/B-VI libraries are used for the HBR-2 benchmark analysis.

# CONTENTS

ABSTRACT ..... iii
FIGURES ..... vii
TABLES ..... ix
ACKNOWLEDGMENTS ..... xi

1 BENCHMARK DEFINITION ..... 1
1.1 INTRODUCTION ..... 1
1.2 DESCRIPTION ..... 2
1.3 CORE POWER DISTRIBUTION AND POWER HISTORY ..... 3
1.4 DOSIMETRY ..... 4
1.5 REFERENCES ..... 5

2 BENCHMARK ANALYSIS ..... 26
2.1 METHODOLOGY ..... 26
2.2 RESULTS AND DISCUSSION ..... 29
2.3 REFERENCES ..... 33

3 CONCLUSIONS ..... 34

APPENDIX A
COMPARISON OF APPROXIMATIONS FOR MODELING THE REACTION RATE VARIATIONS DUE TO CORE POWER REDISTRIBUTION AND COMPARISON OF RESULTS OBTAINED WITH ENDF/B-IV AND ENDF/B-VI CROSS SECTIONS ..... 35
APPENDIX A REFERENCES ..... 42

APPENDIX B
CALCULATED NEUTRON SPECTRA AT THE DOSIMETRY LOCATIONS ..... 43

## FIGURES


1.1 Horizontal cross section of the HBR-2 reactor ........ 12
1.2 Schematic sketch of the axial geometry ........ 13
1.3 Core baffle geometry ........ 14
1.4 Sketch of the surveillance capsule mounting on the thermal shield ........ 15
1.5 The numbering of the fuel elements in the HBR-2 core ........ 16
1.6 Content and format of the FILE1.DAT ........ 17
1.7 Content and format of the FILE2.DAT ........ 18
1.8 Content and format of the FILE3.DAT ........ 19
1.9 Content and format of the FILE4.DAT ........ 20
1.10 Content and format of the FILE5.DAT ........ 21
1.11 Content and format of the FILE6.DAT ........ 22
1.12 Content and format of the FILE7.DAT ........ 23
1.13 Content and format of the FILE8.DAT ........ 24
1.14 Schematic drawing of the axial positions of the cavity dosimeters ........ 25
B.1 Multigroup neutron spectrum, calculated with BUGLE-96 library, in the surveillance capsule ........ 49
B.2 Comparison of multigroup neutron spectra, calculated with different cross-section libraries, in the surveillance capsule ........ 49
B.3 Multigroup neutron spectrum, calculated with BUGLE-96 library, at the position of cavity dosimeters ........ 50
B.4 Comparison of multigroup neutron spectra, calculated with different cross-section libraries, at the position of cavity dosimeters ........ 50

## TABLES

1.1 Selected general data and dimensions of the H. B. Robinson Unit 2 . . . 6
1.2 Materials of the components and regions . . . 8
1.3 Densities and chemical compositions of reactor component materials . . . 10
1.4 Measured specific activities of the dosimeters from the surveillance capsule and from the cavity, at the end of cycle 9 . . . 11
2.1 Reaction rates calculated for the cycle-average power distribution and core power of 2300 MW (100% of nominal power), with different cross-section libraries for transport calculations . . . 29
2.2 Calculated specific activities . . . 30
2.3 Ratios of calculated-to-measured (C/M) specific activities . . . 31
A.1 Ratios of calculated-to-measured (C/M) specific activities obtained with different approximations for the time-dependent variations of reaction rates . . . 40
A.2 Comparison of the C/M ratios of specific activities from the present analysis with the values from the previous analyses . . . 41
B.1 Calculated multigroup neutron fluxes in the surveillance capsule . . . 45
B.2 Calculated multigroup neutron fluxes at the location of cavity dosimeters . . . 47

## ACKNOWLEDGMENTS

The authors wish to thank C. S. Hinnant, R. M. Krich, and W. K. Cantrell of Carolina Power and Light Company, who provided the core depletion calculations for cycle 9 of the H. B. Robinson Unit-2 to supply us with the core power distributions. This work could not have been completed without their kind cooperation. The authors wish to express their appreciation to the reviewers, J. V. Pace III from the Oak Ridge National Laboratory and W. K. Cantrell of Carolina Power and Light Company, for their comments and suggestions. Special thanks go to D. M. Counce, C. I. Moser, and C. H. Shappert for providing the editorial review, and to T. R. Henson and M. R. Whittenbarger for the preparation of this report. Finally, the authors gratefully acknowledge the programmatic support and encouragement from A. Taboada, C. J. Fairbanks, and M. E. Mayfield of the Nuclear Regulatory Commission. Their support was essential for accomplishing our objectives.

# 1 BENCHMARK DEFINITION

## 1.1 INTRODUCTION

This section defines the benchmark for analysis of a power reactor pressure vessel surveillance dosimetry based on data from the H. B. Robinson Unit 2 (HBR-2) power plant. This benchmark will be referred to as the HBR-2 benchmark. Analysis of the HBR-2 benchmark can be used as partial fulfillment of the requirements for the qualification of the methodology for calculating neutron fluence in pressure vessels, as required by the U.S. Nuclear Regulatory Commission Regulatory Guide DG-1053.*

The scope of the HBR-2 benchmark is to validate the capabilities of the calculational methodology to predict the specific activities of the radiometric dosimeters irradiated in a surveillance capsule location (in-vessel) and in a cavity location (ex-vessel), starting from the data that are typically available for an analysis of a power reactor pressure vessel surveillance dosimetry.

The input data provided consist of reactor geometry, material composition, core power distribution, and power history for the time of irradiation. The data given in Section 1 of this document and on the floppy disk accompanying this report are sufficient for the HBR-2 benchmark analysis.† References to other documents are provided but are not necessary for the benchmark calculation.

Experimental data provided are the measured (M) specific activities of the radiometric monitors at the end of irradiation. The dosimeters were irradiated during cycle 9 on the midplane of the HBR-2 core in the surveillance capsule and in the cavity location.

The principal results required from the benchmark analysis are the calculated (C) specific activities at the end of the cycle and the C/M ratios, for all the measurements provided. The reaction rates as obtained from the transport calculations should also be given. Short descriptions of the method and model used should accompany the numerical results.

The cross-section sets, modeling techniques, and approximations to be used in the HBR-2 benchmark analysis will be selected by the analyst; however, they are essential components of the qualified methodology and must be used in a consistent way.

---

*U.S. Nuclear Regulatory Commission, *Calculational and Dosimetry Methods for Determining Pressure Vessel Neutron Fluence*, Draft Regulatory Guide DG-1053, to be published.

†The description of the core power distribution requires a large amount of data, which are provided on the floppy disk.

## 1.2 DESCRIPTION

HBR-2 is a 2300-MW (thermal) pressurized light-water reactor (PWR) designed by Westinghouse and placed in operation in March of 1971. It is owned by Carolina Power and Light Company. The data presented in this section were obtained from Refs. 1 and 2, and from personal communications.[‡,**]

The core of the HBR-2 reactor consists of 157 fuel elements and is surrounded by the core baffle, core barrel, thermal shield, pressure vessel, and biological shield. Selected general data and dimensions of the HBR-2 reactor are given in Table 1.1. An octant of the horizontal cross-section of the reactor is shown schematically in Fig. 1.1, which also shows the locations of the capsule and cavity dosimeters. Axial geometry and dimensions are given in Fig. 1.2. The core baffle geometry is further specified in Fig. 1.3. Surveillance capsules are located in the downcomer region and are attached to the thermal shield. The details of the capsule mounting are shown in Fig. 1.4.

The reactor cavity is 17.10 cm (6.73 in.) wide, measured from the pressure vessel outer radius to the inner radius of the cylindrical biological (concrete) shield. A 7.62-cm (3-in.) thick insulation is installed in the cavity, leaving a 1.31-cm (0.52-in.) air gap between the pressure vessel and the insulation and an 8.18-cm (3.22-in.) air gap between the insulation and the concrete shield. The insulation consists of three steel sheets and eight steel foils with air gaps between them. The total thickness of the insulation steel sheets and foils is 0.2286 cm (0.090 in.). There are two relatively wide (38 cm, or 15 in.) and deep (80.645 cm, or 2 ft, 7.75 in.) detector wells at 0° and 45° azimuthal locations. In each well is a vertical cylinder with a 19.05-cm (7.5-in.) outer diameter and 0.635-cm (0.25-in.)-thick steel wall. The vertical axis of the cylinder is at 252.174 cm (8 ft, 3.28125 in.) from the core center. The concrete surfaces of the detector well are covered with a 0.635-cm (0.25-in.)-thick steel liner. Other concrete surfaces are bare.

The material composition of the reactor components (e.g., pressure vessel, thermal shield, etc.) is given in Table 1.2. Some components (e.g., fuel elements), have an elaborate design, but they are usually approximated as homogenized regions in the transport calculations of the out-of-the-core neutron field. To reduce the amount of data needed for such regions, the volume fractions of the materials are given in Table 1.2. The regions given in Table 1.2 correspond to the ones shown in Figs. 1.1 and 1.2. The core-average water temperature during cycle 9 was ~ 280°C (536°F), and the temperature of the water in the downcomer was approximately 267°C (512°F).[‡] The pressure was 15.513 MPa (2250 psia). The cycle average boron concentration in the coolant was approximately 500 ppm. The corresponding water densities in different regions are also given in Table 1.2. The

---

[‡]S. L. Anderson, Westinghouse Electric Corporation, personal communication to I. Remec, Oak Ridge National Laboratory, 1996.

[**]R. M. Kirch, H. B. Robinson Steam Electric Plant, Unit No. 2, response to request for information regarding operating cycle 9, personal communication to J. V. Pace, Oak Ridge National Laboratory, Oct. 1, 1996.

densities and chemical compositions of the other materials are given in Table 1.3. The concrete of the biological shielding is assumed to be type 02-B ordinary concrete (Ref. 3) with water content reduced to 4.67% by weight and iron concentration increased to reflect an estimated 0.7% by volume addition of rebar (Ref. 1).

## 1.3 CORE POWER DISTRIBUTION AND POWER HISTORY

The fuel assemblies in the core are numbered as shown in Fig. 1.5. These numbers are used in the description of the core power distribution during cycle 9. The data files referred to in the following discussion are provided as ASCII files on the floppy disk.

For each assembly in the core, the mass of uranium, burnup at the beginning of cycle life (BOL) and end of cycle life (EOL), burnup increment in cycle 9, and cycle-average relative power are listed in the data file FILE1.DAT. Part of the file is shown in Fig. 1.6. These data were taken from the TOTE output, except for the cycle-average assembly power. It was calculated from the BOL and EOL assembly-average burnup, taking into account the assembly uranium content. Assembly powers are normalized to the core-wise average of 1.00.

Cycle-average, assembly-wise axial power distributions are given in FILE2.DAT. Part of FILE2.DAT is shown in Fig 1.7. Each assembly is divided vertically into 12 equal-length segments, covering the active length of the fuel, with the first segment on the top and the twelfth segment at the bottom. Cycle-average relative power for each segment is given. Assembly segment powers are normalized to the average value 1.00. Relative powers of the segments were calculated from the relative cumulative axial burnup distributions given in the TOTE output for each assembly.

The cycle-average assembly-pin-power distributions are given in FILE3.DAT. The content of the file is illustrated in Fig. 1.8. Distributions are given for the assemblies in the top right quadrant of the core (e.g., assemblies 2, 3, 7, 8, 9, 10, ... ,79, 80, 81, 82, 83, 84, 85, 86) only. For each assembly, an array of 15 × 15 relative pin powers is given. Pin powers are normalized so that the average of the fuel-pin powers (e.g., 204 per assembly) is 1.00. The pin powers are ordered in rows: the first value corresponds to the pin in the top left corner of the assembly, the last value in row 1 to the pin at the top right corner of the assembly, and the last value in row 15 to the pin at the bottom right corner of the assembly. The orientation of the assembly in the core is as shown in Fig. 1.5. The cycle-average pin powers were obtained by weighting the pin powers which were given at eight core burnup steps during the cycle. The weight assigned to the power distribution at the $I$-th burnup step was proportional to the burnup increment from the midpoint of the $(I-1)$-th and $I$-tn burnup step and $I$-th and $(I+1)$-th burnup step.

For cycle 9, a low-leakage core loading pattern was used in which 12 previously burned fuel elements (i.e., elements number 1, 2, 3, 57, 71, 72, 86, 87, 101, 155, 156, and 157) were put on the core periphery. During cycle 9, the relative powers of the outer assemblies changed significantly. This effect, which is often referred to as power redistribution, is caused by the fuel burnout and gradual changes of the boron concentration in the coolant during the cycle. The power redistribution affects the core neutron leakage and consequently the dosimeter reaction rates. For this reason, the cycle-average core power distribution data, described previously, are supplemented by the power distribution data at several burnup steps during the cycle. At the core-average cycle burnups of 147, 417, 1632, 3363, 5257, 7595, 9293, and 10379 megawatt days per metric ton of uranium (MWd/MTU) the following information is provided: average assembly powers (FILE4.DAT, see Fig. 1.9), assembly burnups (FILE5.DAT, see Fig. 1.10), pin-power distributions for the assemblies in the upper left quadrant of the core (FILE6.DAT, see Fig. 1.11), and assembly-wise axial power distributions in 12 axial segments (FILE7.DAT, see Fig. 1.12).

The core power history for cycle 9 is given in the FILE8.DAT as is illustrated in Fig. 1.13.

Descriptions of the contents and formats of the files are given at the end of each file and are shown in Figs. 1.6–1.13.

## 1.4 DOSIMETRY

During cycle 9, comprehensive sets of dosimeters were irradiated in the surveillance capsule position and in several locations in the reactor cavity (Ref. 2). For the benchmark, a subset of the measurements was chosen. The selected subset consists of the threshold radiometric monitors from the surveillance capsule at the azimuthal angle of 20° and from the cavity dosimetry located at the azimuthal angle of 0°.

A specially built surveillance capsule containing no metallurgical specimens, but otherwise identical to a standard Westinghouse capsule, was placed in a previously used holder at the 20° azimuthal angle location in the downcomer. The region that usually contains metallurgical specimens was filled with carbon steel, and the dosimeters were installed in the holes drilled in the steel. Specific activities given in Table 1.4 are for the core-midplane set.[††] Radially, the dosimeters were installed at the capsule centerline at the radius of 191.15 cm (see Fig. 1.4). The specially built capsule was irradiated during cycle 9 only.

---

[††]Dosimetry sets were installed in the capsule at the core midplane and approximately 28 cm (11 in.) above and below the midplane. The measured activities showed axial variations of only ~ 3%, which is not considered important, and therefore only the results for the midplane set are given.

Specific activities of the cavity dosimeters irradiated at 0° azimuth, on the core midplane,‡‡ are also given in Table 1.4. The dosimeters were irradiated in an aluminum 6061 holder 5.08 cm (2 in.) wide, 1.422 cm (0.56 in.) thick, and 15.240 cm (6 in.) long. Aluminum was selected as the holder material in order to minimize neutron flux perturbations at the dosimeter locations. The holder was supported by a 0.813-mm (0.032-in.)-diam. stainless steel gradient wire mounted vertically in the gap between the insulation and the biological shield at a radius of 238.02 cm (93.71 in.). The sketch of the 0° azimuth cavity dosimetry axial locations is given in Fig. 1.14.

Specific activities listed in Table 1.4 are as-measured with no corrections (e.g., for impurities or photofission). The corrections, which were estimated and used in a previous analysis (Ref. 1) are given in the footnotes to Table 1.4; however, their use is left to the analyst. The specific activities are given for the end of HBR-2 cycle 9 (January 26, 1984, at 12 P.M.).

## 1.5 REFERENCES


1. R. E. Maerker, "LEPRICON Analysis of the Pressure Vessel Surveillance Dosimetry Inserted into H. B. Robinson-2 During Cycle 9," *Nuc. Sci. Eng.*, 96:263 (1987).

2. E. P. Lippincott et al., *Evaluation of Surveillance Capsule and Reactor Cavity Dosimetry from H. B. Robinson Unit 2, Cycle 9*, NUREG/CR-4576 (WCAP-11104), Westinghouse Corp., Pittsburgh, Pa., February 1987.

3. *Reactor Physics Constants*, 2nd ed., ANL-5800, p.600, Argonne National Laboratory, 1963.


---

‡‡In the present benchmark, only the midplane measurements are considered. However, at the 0° azimuth multiple dosimeter sets were irradiated at the midplane and at 213 cm (7 ft) and 107 cm (3.5 ft) above and below the midplane; and activities of the gradient wire [$^{54}Fe(n,p)^{54}Mn$ and $^{58}Ni(n,p)^{58}Co$ reactions] were measured at several positions between the foil locations. Adding these measurements to the benchmark would enlarge the scope of the benchmark to include verification of the calculational methodology for off-midplane locations.

Table 1.1 Selected general data and dimensions of the H. B. Robinson Unit 2

| | | |
|---|---|---|
| **Plant** | | |
| Location | South Carolina, Hartsville | |
| Owner | Carolina Power and Light | |
| Beginning of operation | March 1971 | |
| **Reactor** | | |
| Vendor | Westinghouse | |
| Type | PWR | |
| Coolant | $H_2O$ | |
| Number of loops | 3 | |
| Thermal power | 2300 MW | |
| **Core** | | |
| Number of fuel assemblies | 157 | |
| Pitch | 21.504 cm | 8.466 in. |
| **Fuel Element** | | |
| Type | 15 × 15 array of fuel pins | |
| Fuel pins per element | 204 | |
| Horizontal cross section (including gap) | rectangular, 21.504 cm × 21.504 cm | |
| Height of fuel | 365.76 cm | 12 ft. |
| **Core Baffle*** | | |
| Dimensions | See Fig. 1.3 | |
| Thickness | 2.858 ± 0.013 cm | 1.125 ± 0.005 in. |
| **Core Barrel†** | | |
| Inner radius | 170.023 ± 0.318 cm | 66.938 ± 0.125 in. |
| Thickness | 5.161 ± 0.107 cm | 2.032 ± 0.042 in. |
| **Thermal Shield** | | |
| Inner radius | 181.135 ± 0.318 cm | 71.313 ± 0.125 in. |
| Thickness | 6.825 ± 0.160 cm | 2.687 ± 0.063 in. |
| **Pressure Vessel** | | |
| Cladding | | |
| Inner radius | 197.485 ± 0.076 cm | 77.750 ± 0.030 in. |
| Thickness (minimal) | 0.556 cm | 7/32 in. (0.219 in.) |
| Base metal | | |
| Inner radius‡ | 198.041 cm | 77.969 in. |
| Thickness** | 23.614 ± 0.041 cm | 9.297 ± 0.016 in. |
| Total thickness (wall + cladding ) | 24.170 cm | 9.516 in. |

**Table 1. 1 (continued)**

| | | |
|---|---|---|
| **Pressure Vessel Thermal Insulation** | | |
| Inner radius | 222.964 cm | 87.781 in. |
| Total insulation thickness (including voids) | 7.620 cm | 3.0 in. |
| Insulation steel components | | |
| 1 steel sheet | 0.079 cm | 0.031 in. |
| 1 steel sheet | 0.046 cm | 0.018 in. |
| 1 steel sheet | 0.064 cm | 0.025 in. |
| 8 steel foils | 0.005 cm | 0.002 in. |
| Total thickness of the steel in the insulation | 0.229 cm | 0.090 in. |
| **Pressure Vessel Cavity** | See Fig. 1.1 | |
| Dimensions | | |
| Vessel-to-insulation gap | 1.31 cm | 0.52 in. |
| Insulation | 7.62 cm | 3.00 in. |
| Insulation-to-concrete gap | 8.18 cm | 3.22 in. |
| Total width of the cylindrical part | 17.10 cm | 6.73 in. |
| **Biological Shield** | | |
| Dimensions | See Fig. 1.1 | |
| Inner radius of cylindrical surfaces | 238.760 cm | 7 ft 10 in. |

* The baffle units are positioned symmetrically about the core center within 0.025 cm (0.010 in.) measured at the top and bottom former elevations.

† The annular gap between the core barrel outer radius and the thermal shield inner radius is maintained uniform within 0.381 cm (0.150 in.).

‡ The pressure vessel base metal inner radius is obtained as the cladding inner radius plus specified minimum cladding thickness of 0.556 cm (7/32 in.).

** The pressure vessel thickness is based on a single measurement of the lower shell and three measurements of the intermediate shell (S. L. Anderson, Westinghouse Electric Corporation, personal communication to I. Remec, Oak Ridge National Laboratory, 1996).

**Table 1.2 Materials of the components and regions**

| Region | Material* | Volume fraction |
|---|---|---|
| **Reactor core** | $UO_2$, enriched to 2.9%, density 10.418 g $cm^{-3}$ | 0.2997 |
| | Zircaloy-4 | 0.1004 |
| | Inconel-718 | 0.00281 |
| | Stainless steel SS-304 | 0.00062 |
| | Water density 0.766 g $cm^{-3}$ | 0.5886 |
| **Core baffle** | Stainless steel SS-304 | 1.00 |
| **Bypass region** | Water density 0.776 g $cm^{-3}$ | See Fig. 1.2 |
| **Core barrel** | Stainless steel SS-304 | 1.00 |
| **Downcomer region No. 1** | Water density 0.787 g $cm^{-3}$ | 1.00 |
| **Thermal shield** | Stainless steel SS-304 | 1.00 |
| **Surveillance capsule** | | |
| Mounting | Stainless steel SS-304 | 1.00 |
| Content | Steel A533B | 1.00 |
| **Downcomer region No. 2** | Water density 0.787 g $cm^{-3}$ | 1.00 |
| **Pressure vessel cladding** | Stainless Steel SS-304 | 1.00 |
| **Pressure vessel** | Steel A533B | 1.00 |
| **Insulation** | Stainless steel SS-304 | 0.03 |
| | Air | 0.97 |
| **Reactor cavity** | Air | 1.00 |
| **Biological shield** | Concrete | 1.00 |

**Table 1.2 (continued)**

| Region | Material | Volume Fraction |
|---|---|---|
| **Core support** | Stainless steel SS-304<br>Water<br>density 0.787 g cm | 0.049<br>0.951 |
| **Lower core plate** | Stainless steel SS-304<br>Water<br>density 0.787 g $cm^{-3}$ | 0.668<br>0.332 |
| **Nozzle legs** | Stainless steel SS-304<br>Water<br>density 0.787 g $cm^{-3}$ | 0.070<br>0.930 |
| **Bottom nozzle plate** | Stainless steel SS-304<br>Water<br>density 0.787 g $cm^{-3}$ | 0.717<br>0.283 |
| **Water gap No. 1** | Stainless steel SS-304<br>Water<br>density 0.787 g $cm^{-3}$ | 0.007<br>0.993 |
| **End plugs** | Stainless steel SS-304<br>Water<br>density 0.787 g $cm^{-3}$ | 0.300<br>0.700 |
| **Fuel plenum** | Stainless steel SS-304<br>Water<br>density 0.745 g $cm^{-3}$ | 0.224<br>0.560 |
| **Water gap No.2** | Stainless steel SS-304<br>Water<br>density 0.745 g $cm^{-3}$ | 0.017<br>0.983 |
| **Top nozzle** | Stainless steel SS-304<br>Water<br>density 0.745 g $cm^{-3}$ | 0.275<br>0.725 |
| **Formers** | Stainless steel SS-304<br>Water<br>density 0.766 g $cm^{-3}$ | 0.900<br>0.100 |

* The boron concentration in the coolant was approximately 500 ppm (cycle average).

Table 1.3 Densities ($gcm^{-3}$) and chemical compositions (wt %) of reactor component materials

| | Carbon steel A533B | Stainless steel SS-304 | Inconel-718 | Zircaloy-4 | Concrete* |
|---|---|---|---|---|---|
| **Density** | 7.83 | 8.03 | 8.3 | 6.56 | 2.275 |
| **Element** | | | | | |
| Fe | 97.90 | 69.0 | 7.0 | 0.50 | 3.82 |
| Ni | 0.55 | 10.0 | 73.0 | | |
| Cr | | 19.0 | 15.0 | | |
| Mn | 1.30 | 2.0 | | | |
| C | 0.25 | | | | 0.10 |
| Ti | | | 2.5 | | |
| Si | | | 2.5 | | 34.09 |
| Zr | | | | 97.91 | |
| Sn | | | | 1.59 | |
| Ca | | | | | 4.40 |
| K | | | | | 1.31 |
| Al | | | | | 3.43 |
| Mg | | | | | 0.22 |
| Na | | | | | 1.62 |
| O | | | | | 50.50 |
| H | | | | | 0.51 |

* The concrete is assumed to be type 02-B ordinary concrete (Ref. 3) with water content reduced to 4.67% by weight and iron concentration increased to reflect an estimate 0.7% by volume addition of rebar (Ref. 1).

**Table 1.4 Measured specific activities of the dosimeters from the surveillance capsule and from the cavity, at the end of cycle 9 (1/26/1984).** Specific activities (Bq/mg) are given per mg of Ni, Fe, Ti, and Cu material with naturally occurring isotopic composition, and per mg of $^{237}$Np and $^{238}$U isotopes.

| Dosimeter | Surveillance capsule (core midplane, 20° azimuth, radius 191.15 cm)* | Cavity (core midplane, 0° azimuth, radius 238.02 cm)† |
|---|---|---|
| $^{237}$Np($n,f$) $^{137}$Cs | $3.671 \times 10^{2}$ | $2.236 \times 10^{1}$ |
| $^{238}$U($n,f$) $^{137}$Cs | $5.345 \times 10^{1}$ | $8.513 \times 10^{-1}$ |
| $^{58}$Ni ($n,p$) $^{58}$Co | $1.786 \times 10^{4}$‡ | $1.959 \times 10^{2}$ |
| $^{54}$Fe ($n,p$) $^{54}$Mn | $9.342 \times 10^{2}$‡ | 8.711 |
| $^{46}$Ti ($n,p$) $^{46}$Sc | $3.500 \times 10^{2}$** | 3.310 |
| $^{63}$Cu ($n,\alpha$) $^{60}$Co | $2.646 \times 10^{1}$** | $2.645 \times 10^{-1}$ |

* Dosimeters in the capsule were irradiated under 0.508 mm (0.020 in.) Gd cover, except where noted differently. Ref. 1 estimates that in order to compensate for the photofission contribution, the $^{137}$Cs activity in $^{237}$Np and $^{238}$U should be reduced by 2.5% and 5%, respectively; and $^{60}$Co activity in $^{63}$Cu should be reduced by 2.5% to compensate for the contribution from the $^{59}$Co($n,\gamma$)$^{60}$Co reaction on the Co impurities in the Cu dosimeter.

† In the cavity, the $^{237}$Np, $^{238}$U, and Ni dosimeters were irradiated under 0.508 mm (0.020 in.) Cd cover. Ti and Fe dosimeters were irradiated bare. Activity of the Fe is an average of four measurements. The Cu activity is an average of one bare dosimeter and one dosimeter irradiated in Cd cover. Ref. 1 estimates that in order to compensate for the photofission contribution, the $^{137}$Cs activity in $^{237}$Np and $^{238}$U should be reduced by 5.0% and 10.0%, respectively; and $^{60}$Co activity in $^{63}$Cu should be reduced by 2.5% to compensate for the contribution from the $^{59}$Co($n,\gamma$)$^{60}$Co reaction on the Co impurities in the Cu dosimeter.

‡ Average of five dosimeters, three inside Gd and two outside.

** Average of two measurements.

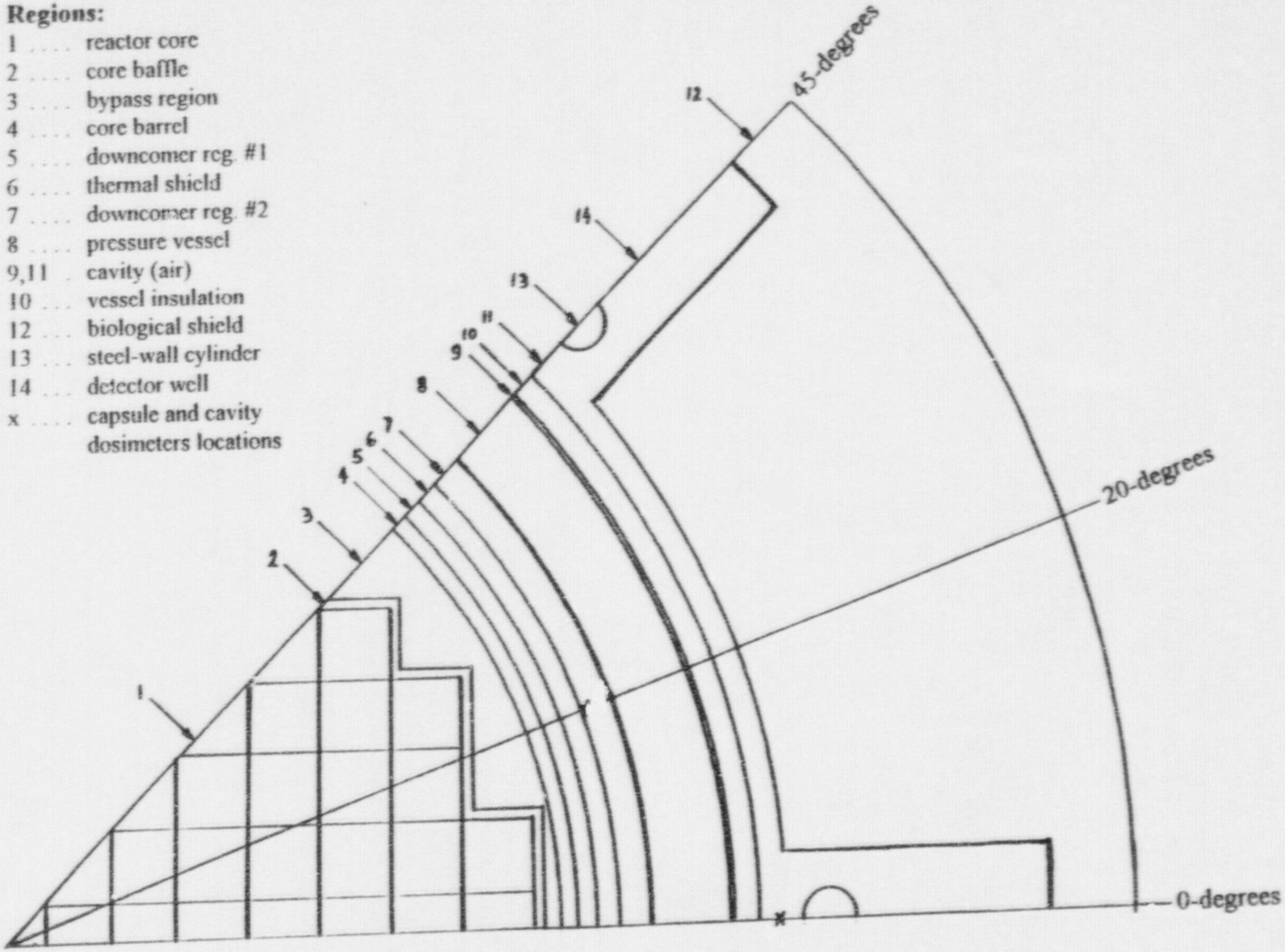


**Fig. 1.1 Horizontal cross section of the HBR-2 reactor.** One octant of the core is shown

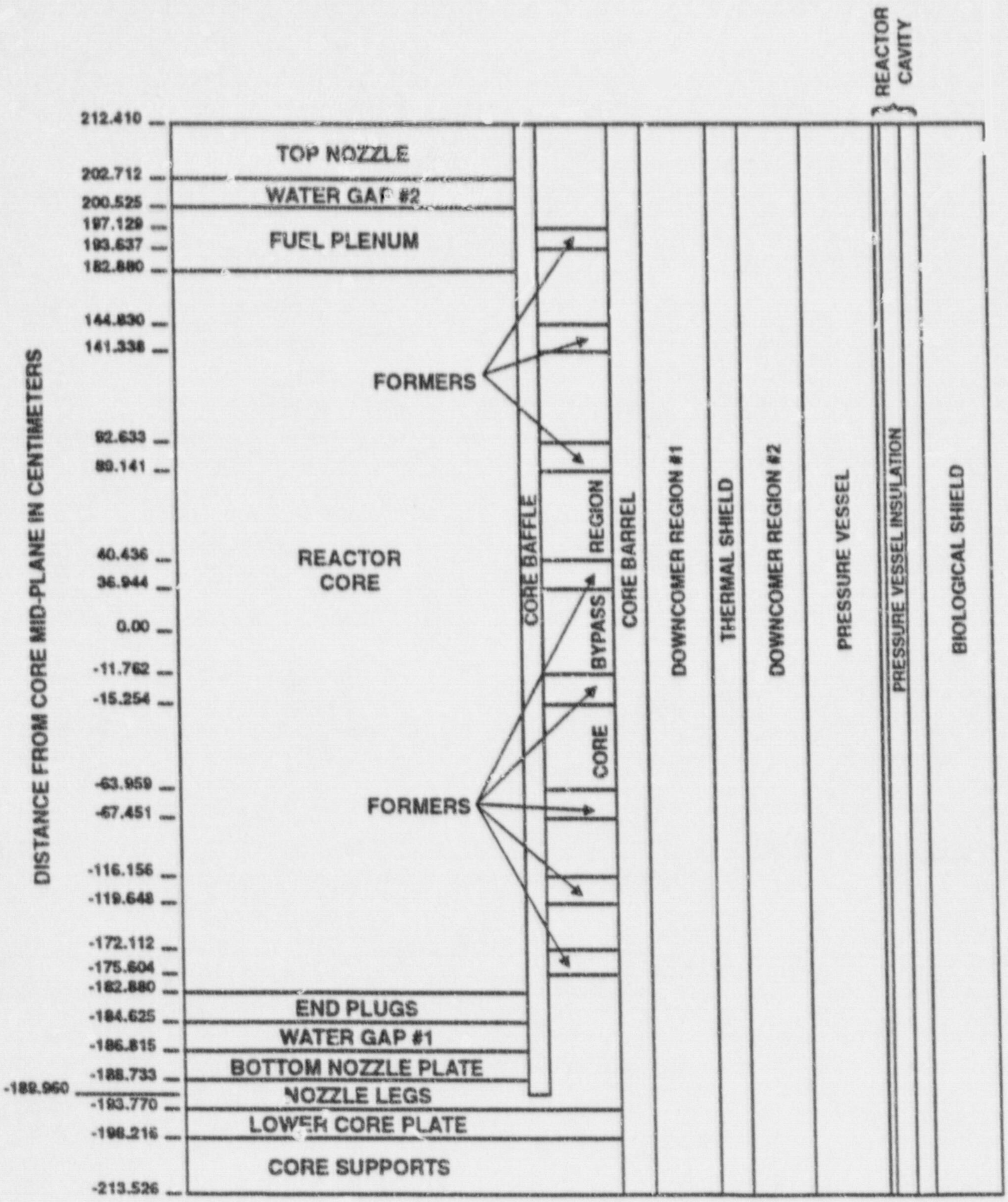


Fig. 1.2 Schematic sketch of the axial geometry (not to scale). Dimensions are in centimeters

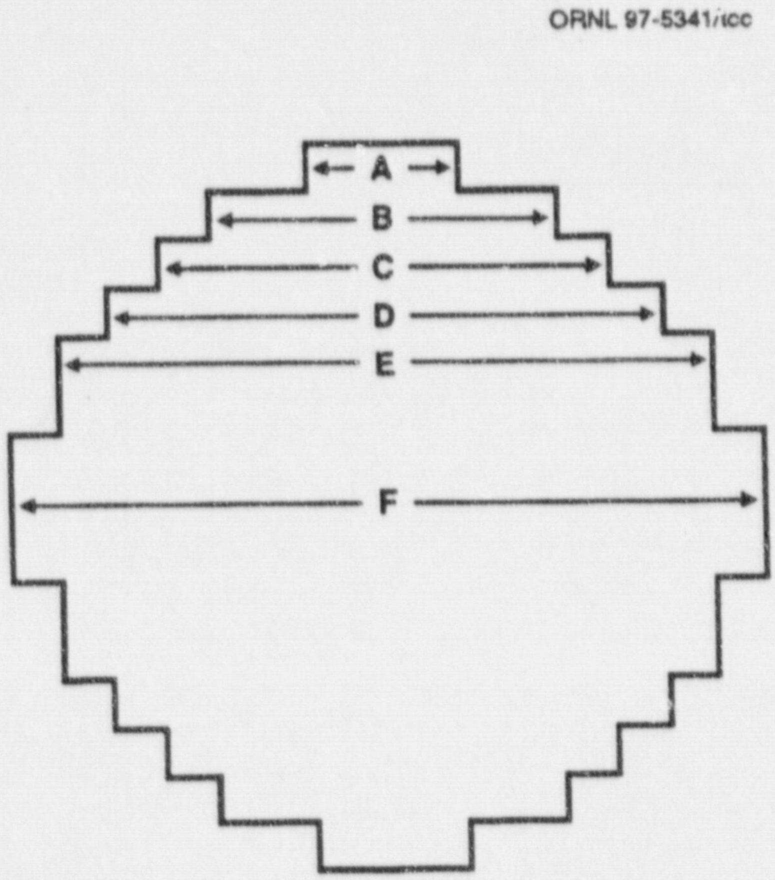


| | DIMENSION | |
|---|---|---|
| A | 64.607 ± 0.036 cm | (25.436 ± 0.014 in.) |
| B | 150.663 ± 0.046 cm | (59.316 ± 0.018 in.) |
| C | 193.680 ± 0.056 cm | (76.252 ± 0.022 in.) |
| D | 236.698 ± 0.066 cm | (93.188 ± 0.026 in.) |
| E | 279.715 ± 0.076 cm | (110.124 ± 0.030 in.) |
| F | 322.684 ± 0.084 cm | (127.041 ± 0.033 in.) |

**Fig. 1.3 Core baffle geometry.** Nominal dimensions are given for the core-side surfaces of the baffle plates. Deviations from nominal are for the maximum and minimum dimensions (e.g., for A the nominal dimension is 64.607 cm, with the maximum value of 64.643 cm and the minimum value of 64.571 cm)

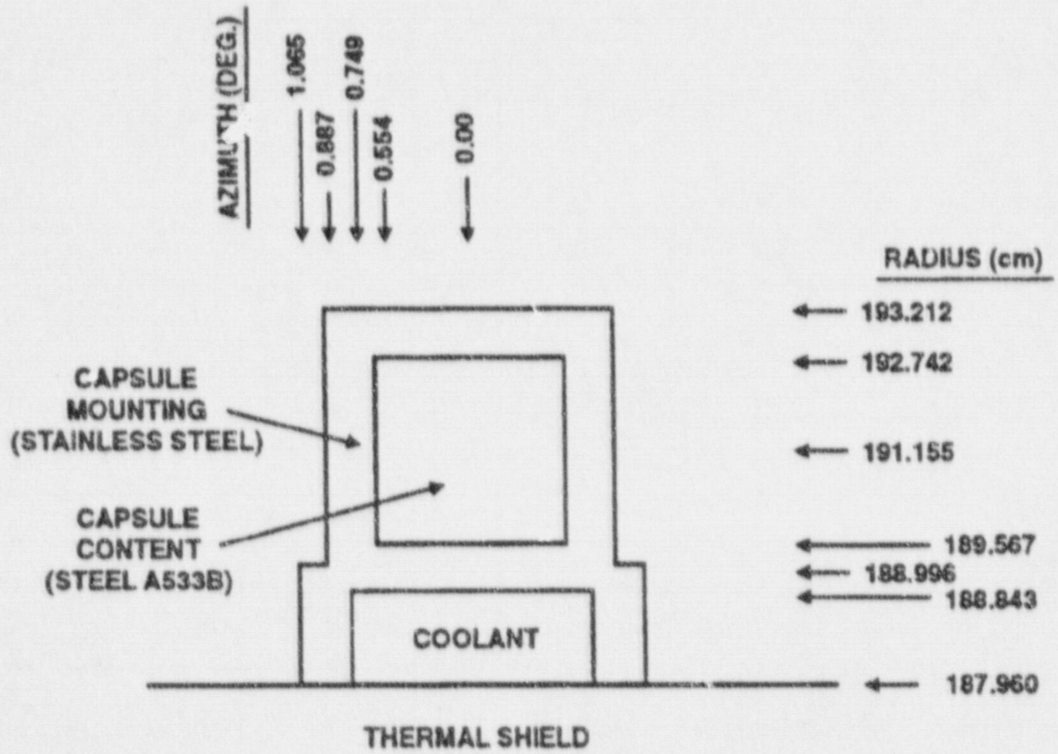


**Fig. 1.4 Sketch of the surveillance capsule mounting on the thermal shield (not to scale).** The capsule centerline is at 191.155 ± 0.152 cm (75.258 ± 0.060 in.) (S. L. Anderson, Westinghouse Electric Corporation, personal communication to I. Remec, Oak Ridge National Laboratory, 1996)

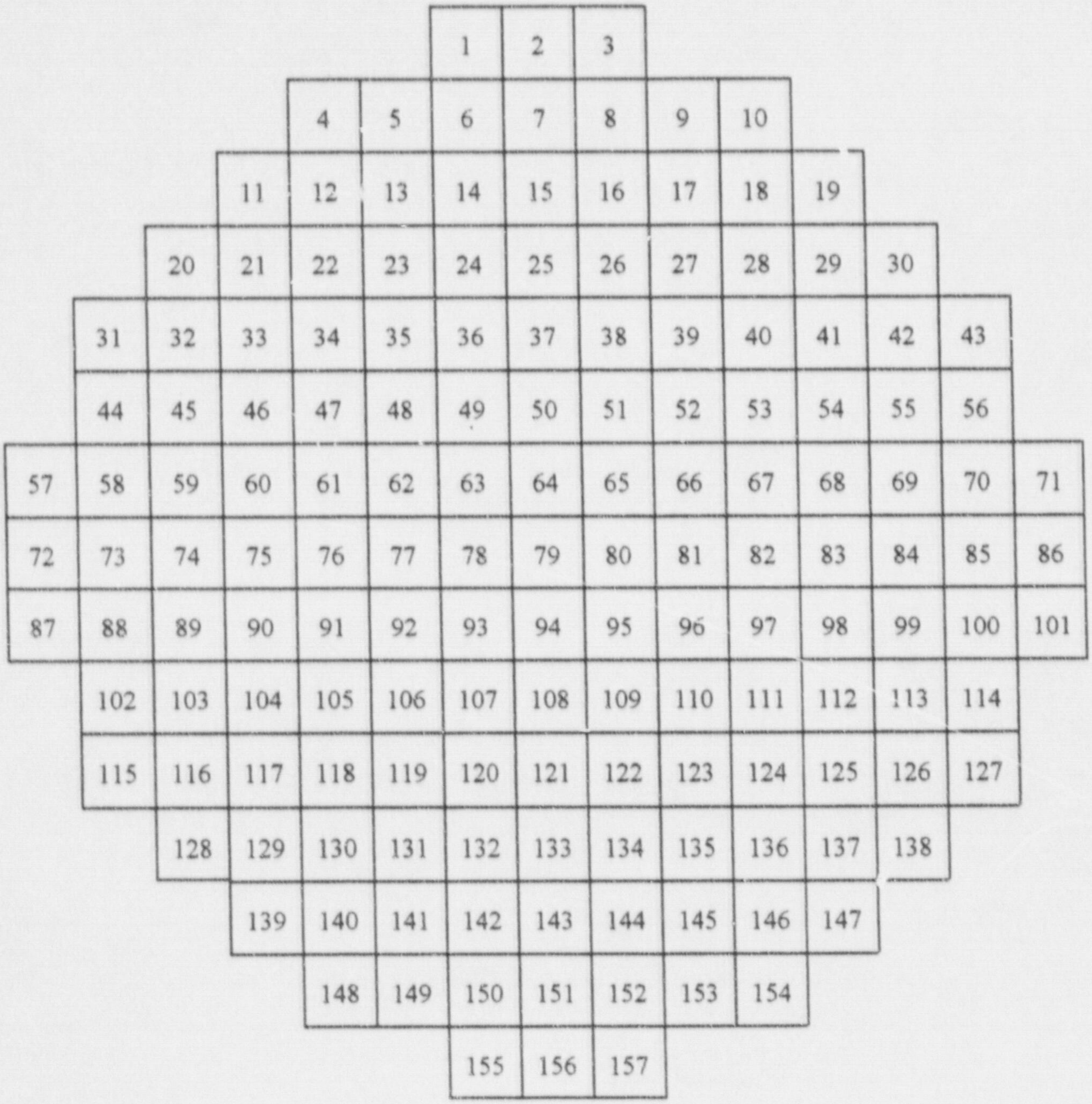


**Fig. 1.5 The numbering of the fuel elements in the HBR-2 core**

```
ASS. #    MTU      BU-BOL   BU-EOL     dBU      Ave. P
    1   0.4285    29488.   33102.    3614.     0.337
    2   0.4269    22091.   26798.    4707.     0.438
    3   0.4288    29122.   32688.    3566.     0.333
                              .
                              .
                              .
  155   0.4285    29057.   32748.    3691.     0.345
  156   0.4281    22727.   27443.    4716.     0.440
  157   0.4291    29270.   32842.    3572.     0.334
EOF

Legend:
ASS. #.....assembly number as in Fig. 1.5.
MTU........mass of uranium in the assembly
           in metric tonnes.
BU-BOL.....assembly burnup in MWd/MTU at the beginning
           of cycle (BOL).
BU-EOL.....assembly burnup in MWd/MTU at the end of
           cycle (EOL).
dBU........assembly burnup increase in cycle 9 in
           MWd/MTU.
Ave. P.....cycle-average assembly power.

Format: (I5,F9.4,3F9.0,F9.3)
```

**Fig. 1.6 Content and format of the FILE1.DAT.** Beginning and end of file are shown

```
ASS. #  Cycle-average, assembly axial-segment-powers

  1 0.696895 0.995964 1.064975 1.054674 1.076852 1.063509
    1.087683 1.073097 1.090714 1.071349 1.012495 0.711793
  2 0.690069 0.992619 1.064409 1.053981 1.080842 1.062351
    1.092513 1.074481 1.088941 1.070761 1.012128 0.716907
  3 0.597160 0.942708 1.056286 1.058032 1.084421 1.075771
    1.101560 1.090651 1.100337 1.093457 1.032470 0.767144
                                 .
                                 .
                                 .
155 0.766128 1.028479 1.076598 1.088410 1.084673 1.077273
    1.102337 1.077251 1.093745 1.056529 0.955013 0.593564
156 0.695985 0.991515 1.066876 1.080861 1.088512 1.080346
    1.104275 1.084720 1.098602 1.071259 0.984913 0.652136
157 0.572353 0.931786 1.054233 1.069350 1.094944 1.084444
    1.106110 1.094919 1.103209 1.094470 1.029888 0.764293
EOF
```

**Legend:**
Ass. # ........assembly number as in Fig. 1.5.

Cycle-average, assembly axial-segment powers (12 segments per assembly) are relative powers of axial segments of the assembly. Each segment is 30.48 cm long (1 ft). First segment (after Ass. #) is at the top of active fuel and last segment is at the bottom of the fuel. Normalization is to the average segment power of 1.00 in every assembly (e.g., the sum of segment powers in any assembly is 12).

**Format:** (I3,6F9.6/3X,6F9.6)

**Fig. 1.7 Content and format of the FILE2.DAT.** Beginning and end of file are shown

```
CYCLE-AVERAGE PIN POWERS

ASSEMBLY NUMBER    2
  1  .2896  .2963  .3044  .3108  .3162  .3202  .3219  .3224  .3223  .3211  .3173  .3124  .3062  .2985  .2920
  2  .4325  .4446  .4608  .4628  .4693  .4798  .4758  .4721  .4764  .4810  .4710  .4650  .4636  .4476  .4359
  3  .5393  .5615  .0000  .5859  .5935  .0000  .6055  .6004  .6061  .0000  .5956  .5888  .0000  .5654  .5433
  4  .6267  .6441  .6698  .6797  .695   .7006  .7009  .0000  .7017  .7022  .6981  .6830  .6739  .6487  .6312
  5  .7077  .7274  .7561  .7754  .0000  .7768  .7671  .7743  .7680  .7785  .0000  .7791  .7607  .7326  .7128
  6  .7884  .8198  .0000  .8609  .8563  .8428  .8338  .8348  .8347  .8447  .8593  .8650  .0000  .8254  .7938
  7  .8676  .8910  .9323  .9441  .9267  .9137  .9222  .9346  .9231  .9157  .9299  .9485  .9377  .8970  .8735
  8  .9488  .9653 1.0090  .0000 1.0204  .9976 1.0191  .0000 1.0201  .9997 1.0237  .0000 1.0148  .9715  .9549
  9 1.0329 1.0596 1.1076 1.1206 1.0993 1.0834 1.0931 1.1074 1.0941 1.0854 1.1027 1.1255 1.1136 1.0661 1.0391
 10 1.1185 1.1604  .0000 1.2142 1.2061 1.1859 1.1726 1.1736 1.1737 1.1881 1.2096 1.2192  .0000 1.1671 1.1248
 11 1.2009 1.2303 1.2749 1.3039  .0000 1.3016 1.2842 1.2957 1.2853 1.3038  .0000 1.3090 1.2811 1.2371 1.2071
 12 1.2853 1.3149 1.3614 1.3765 1.4047 1.4118 1.4107  .0000 1.4118 1.4141 1.4084 1.3815 1.3677 1.3217 1.2914
 13 1.3729 1.4201  .0000 1.4660 1.4790  .0000 1.5020 1.4883 1.5030  .0000 1.4826 1.4710  .0000 1.4269 1.3788
 14 1.4609 1.4875 1.5288 1.524  1.5369 1.5649 1.5480 1.5343 1.5490 1.5670 1.5403 1.5291 1.5349 1.4940 1.4665
 15 1.5606 1.5704 1.5888 1.6019 1.6130 1.6223 1.6233 1.6233 1.6243 1.6244 1.6163 1.6066 1.5947 1.5768 1.5660

                                              .
                                              .
                                              .

ASSEMBLY NUMBER   86
  1 1.5463 1.4474 1.3604 1.2750 1.1928 1.1120 1.0279  .9449  .8658  .7881  .7084  .6279  .5406  .4339  .2907
  2 1.5542 1.4724 1.4083 1.3042 1.2227 1.1558 1.0563  .9635  .8913  .8222  .7233  .6474  .5657  .4480  .2992
  3 1.5704 1.5138  .0000 1.3520 1.2692  .0000 1.1057 1.0100  .9345  .0000  .7618  .6756  .0000  .4664  .3085
  4 1.5820 1.5068 1.4531 1.3662 1.2985 1.2108 1.1206  .0000  .9481  .8663  .7825  .6866  .5934  .4691  .3158
  5 1.5916 1.5188 1.4666 1.3960  .0000 1.2029 1.0982 1.0222  .9305  .8626  .0000  .7050  .6028  .4770  .3221
  6 1.5989 1.5467  .0000 1.4018 1.2953 1.1818 1.0825  .9997  .9180  .8491  .7857  .7109  .0000  .4893  .3271
  7 1.5978 1.5275 1.4868 1.4016 1.2773 1.1692 1.0930 1.0223  .9277  .8414  .7768  .7131  .6172  .4861  .3296
  8 1.5953 1.5125 1.4736  .0000 1.2895 1.1709 1.1086  .0000  .9415  .8438  .7858  .0000  .6139  .4835  .3309
  9 1.5957 1.5267 1.4870 1.4027 1.2792 1.1716 1.0959 1.0256  .9312  .8452  .7806  .7172  .6210  .4895  .3321
 10 1.5948 1.5450  .0000 1.4041 1.2991 1.1867 1.0883 1.0062  .9251  .8565  .7935  .7187  .0000  .4959  .3320
 11 1.5857 1.5164 1.4673 1.3995  .0000 1.2104 1.1071 1.0322  .9411  .8739  .0000  .7165  .6137  .4666  .3292
 12 1.5742 1.5036 1.4541 1.3708 1.3062 1.2210 1.1327  .0000  .9629  .8813  .7978  .7015  .6076  .4814  .3248
 13 1.5608 1.5098  .0000 1.3577 1.2787  .0000 1.1206 1.0264  .9522  .0000  .7802  .6938  .0000  .4815  .3193
 14 1.5424 1.4674 1.4095 1.3106 1.2334 1.1703 1.0732  .9822  .9116  .8435  .7517  .6684  .5861  .4658  .3121
 15 1.5313 1.4407 1.3609 1.2815 1.2045 1.1278 1.0469  .9663  .8888  .8122  .7331  .6525  .5643  .4551  .3065
EOF
```

**Legend:**
For each assembly in the top right quadrant of the core an array of 15 x 15 relative pin powers p(i,j) is given. The assembly is oriented as in Fig. 1.5, pin(1,1) is in the top left corner, pin(1,15) in the top right corner, pin(15,1) in the bottom left corner and pin(15,15) in the bottom right corner.

For each assembly in the top right quadrant of the core the following is given:

ASSEMBLY NUMBER    #..........assembly number as in Fig. 1.5; one record.
**Format:** (' ASSEMBLY NUMBER  ',I3)

Row number i, pin powers  p(i,j),j=1,15; fifteen records.
**Format:** (I3,15F7.4).

**Fig. 1.8 Content and format of the FILE3.DAT.** Beginning and end of file are shown

```
ASSEMBLY RELATIVE POWERS FOR BURNUP STEP   1 (  147 MWd/MTU)

CORE AVERAGE ASSEMBLY POWER  1.000

                                             .241   .329   .244
                               .705   .874   .853   .910   .855   .876   .707
                        .784  1.180  1.289  1.014   .883  1.016  1.292  1.183   .786
                 .781  1.054  1.190  1.116  1.266   .995  1.269  1.118  1.193  1.058   .784
          .701  1.173  1.181  1.038  1.201  1.028  1.138  1.031  1.207  1.052  1.190  1.177   .703
          .868  1.280  1.108  1.196  1.113  1.258  1.086  1.264  1.120  1.207  1.114  1.183   .867
   .239   .846  1.008  1.260  1.024  1.257  1.171  1.371  1.177  1.263  1.029  1.263  1.007   .842   .235
   .317   .897   .876   .991  1.134  1.082  1.365  1.133  1.374  1.086  1.136   .992   .876   .896   .317
   .239   .844  1.006  1.261  1.027  1.259  1.171  1.367  1.174  1.262  1.027  1.261  1.008   .845   .239
          .868  1.280  1.112  1.203  1.114  1.256  1.082  1.258  1.115  1.198  1.108  1.280   .867
          .702  1.175  1.187  1.047  1.198  1.024  1.131  1.024  1.198  1.036  1.179  1.172   .701
                 .783  1.055  1.187  1.11   1.257   .984  1.256  1.109  1.183  1.050   .780
                        .783  1.177  1.282  1.003   .857  1.002  1.279  1.173   .780
                               .703   .868   .845   .896   .843   .867   .701
                                             .241   .322   .241
                                                      .
                                                      .
                                                      .
ASSEMBLY RELATIVE POWERS FOR BURNUP STEP   8 (10379 MWd/MTU)

CORE AVERAGE ASSEMBLY POWER  1.000

                                             .382   .508   .386
                               .741  1.016  1.184  1.234  1.185  1.016   .741
                        .847  1.121  1.215  1.050   .971  1.051  1.215  1.120   .847
                 .847  1.262  1.135  1.018  1.159   .961  1.158  1.017  1.134  1.262   .847
          .741  1.121  1.132   .969  1.060   .957  1.257   .957  1.060   .975  1.133  1.120   .741
         1.017  1.215  1.016  1.059   .963  1.072   .958  1.073   .964  1.061  1.017  1.214  1.016
   .387  1.188  1.053  1.159   .957  1.072   .950  1.070   .951  1.072   .957  1.159  1.051  1.184   .382
   .514  1.237   .972   .962  1.257   .958  1.068   .869  1.071   .958  1.257   .962   .972  1.237   .514
   .386  1.186  1.051  1.159   .957  1.073   .950  1.069   .951  1.074   .957  1.160  1.053  1.188   .387
         1.017  1.214  1.018  1.062   .965  1.072   .959  1.074   .965  1.060  1.017  1.215  1.018
          .741  1.121  1.134   .975  1.060   .957  1.258   .958  1.061   .970  1.132  1.121   .742
                 .847  1.263  1.135  1.018  1.159   .959  1.159  1.019  1.135  1.263   .848
                        .848  1.122  1.216  1.050   .956  1.049  1.216  1.122   .848
                               .742  1.017  1.185  1.233  1.185  1.018   .742
                                             .380   .504   .386
EOF
```

**Legend:**

Assembly relative powers at eight core burnups.
Assembly relative powers are normalized to
the average core-wise value of 1.00.

**Format:** free format

**Fig. 1.9 Content and format of the FILE4.DAT.** Beginning and end of file are shown

```
CYCLE  9 AT   147.00 MWd/T (MICROBURN-P  CASE  9     RNP Cycle 09 MAP413, 0773 ppm, 1761 MW, 00147 MWd/MTU)
ASSEMBLY BURNUPS IN  1000 MWd/MTU

                                                  29.274  22.141  29.143
                                    .106    .131    .127    .136    .128    .131    .106
                            .117   7.706   6.970  18.806  23.048  18.808   6.947   7.705    .118
                    .117    .158  12.146  19.792   7.328  18.895   7.322  19.800  12.097    .158    .117
            .105   7.715  12.202  21.817  12.075  22.998    .166  22.990  12.071  21.517  12.225   7.717    .105
            .130   7.007  19.815  12.084  19.658  10.232  21.989  10.215  19.658  12.090  19.824   7.001    .130
  29.272    .126  18.796   7.333  23.032  10.252  19.673   8.274  19.676  10.262  23.040   7.337  18.798    .125  29.143
  21.147    .133  23.046  18.893    .166  22.074   8.373  21.264   8.329  22.080    .166  18.894  23.049    .133  21.149
  29.275    .126  18.799   7.340  23.034  10.275  19.673   8.274  19.678  10.259  23.025   7.336  18.800    .126  29.275
            .130   7.040  19.835  12.085  19.655  10.216  21.989  10.230  19.653  12.081  19.835   6.999    .130
            .105   7.718  12.265  21.517  12.069  22.987    .165  22.999  12.074  21.834  12.217   7.717    .105
                    .117    .158  12.103  19.786   7.321  18.898   7.325  19.803  12.138    .157    .117
                            .117   7.704   6.947  18.806  23.045  18.808   6.967   7.705    .117
                                    .105    .130    .126    .133    .126    .130    .105
                                                  29.143  22.775  29.145

                                                          .
                                                          .
                                                          .

CYCLE  9 AT 10379.00 MWd/T (MICROBURN-P  CASE 34     RNP Cycle 09 MAP455, 0040 ppm, 1261 MW, 10379 MWd/MTU)
ASSEMBLY BURNUPS IN  1000 MWd/MTU

                                                  32.497  26.471  32.406
                                   7.376   9.749  10.704  11.323  10.727   9.757   7.380
                           8.430  19.295  19.616  29.438  32.739  29.451  19.604  19.299   8.435
                   8.423  12.298  23.936  30.586  19.817  29.462  19.819  30.593  23.891  12.310   8.428
           7.369  19.285  23.945  31.964  23.464  33.192  13.041  33.199  23.475  31.745  23.999  19.291   7.364
           9.743  19.632  30.575  23.446  30.080  21.956  32.380  21.970  30.110  23.503  30.606  19.620   9.717
  32.528  10.717  29.437  19.817  33.217  21.980  30.281  20.477  30.314  22.011  33.239  19.817  29.407  10.661  32.349
  25.456  11.312  32.733  29.461  13.032  32.449  20.542  31.588  20.551  32.472  13.040  29.462  32.729  11.291  25.446
  32.525  10.689  29.417  19.823  33.235  22.019  30.283  20.461  30.309  22.017  33.226  19.823  29.437  10.709  32.527
           9.737  19.660  30.621  23.497  30.091  21.941  32.371  21.972  30.092  23.463  30.598  19.624   9.741
           7.369  19.296  24.046  31.740  23.446  33.170  13.017  33.188  23.461  31.976  23.954  19.283   7.367
                   8.431  12.313  23.888  30.560  19.775  29.412  19.777  30.575  23.905  12.284   8.418
                           8.433  19.289  19.577  29.390  32.542  29.383  19.586  19.279   8.422
                                   7.371   9.731  10.666  11.240  10.659   9.725   7.366
                                                  32.384  27.050  32.385
EOF
```

**Legend:** Assembly burnups at eight core burnup steps.

**Format:** free format

**Fig. 1.10 Content and format of the FILE5.DAT.** Beginning and end of file are shown

```
PIN POWERS FOR BURNUP STEP #  1 (  147 MWd/MTU)

 ASSEMBLY NUMBER    2
 ASSEMBLY AVERAGE FUEL-ROD POWER BEFORE NORMALIZATION     .329
  1  .2747  .2823  .2908  .2975  .3027  .3069  .3085  .3091  .3088  .3076  .3039  .2990  .2930  .2848  .2775
  2  .4115  .4249  .4416  .4437  .4501  .4607  .4568  .4534  .4574  .4622  .4519  .4461  .4446  .4282  .4151
  3  .5142  .5376  .0000  .5631  .5707  .0000  .5829  .5780  .5838  .0000  .5732  .5662  .0000  .5419  .5188
  4  .5987  .6178  .6443  .6540  .6704  .6756  .6765  .0000  .6774  .6774  .6731  .6576  .6488  .6227  .6039
  5  .6780  .6993  .7291  .7488  .0000  .7516  .7418  .7494  .7427  .7537  .0000  .7[illegible]8  .7342  .7051  .6838
  6  .7565  .7920  .0000  .8351  .8315  .8178  .8099  .8111  .8111  .8199  .8348  .8394  .0000  .7984  .7646
  7  .8391  .8649  .9078  .9208  .9041  .8920  .9008  .9135  .9020  .8944  .9075  .9257  .9138  .8716  .8461
  8  .9236  .9430  .9889  .0000 1.0023  .9804 1.0026  .0000 1.0038  .9825 1.0059  .0000  .9953  .9503  .9309
  9 1.0126 1.0424 1.0828 1.1077 1.0868 1.0719 1.0819 1.0971 1.0831 1.0743 1.0907 1.1132 1.0998 1.0500 1.0199
 10 1.1044 1.1506  .0000 1.2083 1.2016 1.1810 1.1688 1.1700 1.1700 1.1834 1.2059 1.2141  .0000 1.1585 1.1120
 11 1.1946 1.2278 1.2761 1.3068  .0000 1.3071 1.2892 1.3013 1.2904 1.3098  .0000 1.3129 1.2834 1.2357 1.2022
 12 1.2889 1.3232 1.3739 1.3898 1.4208 1.4290 1.4287  .0000 1.4299 1.4317 1.4250 1.3955 1.3815 1.3314 1.2968
 13 1.3913 1.4445  .0000 1.4964 1.5110  .0000 1.5359 1.5220 1.5371  .0000 1.5153 1.5025  .0000 1.4527 1.3989
 14 1.5019 1.5347 1.5806 1.5773 1.5909 1.6222 1.6040 1.5903 1.6052 1.6250 1.5952 1.5830 1.5682 1.5429 1.5095
 15 1.6411 1.6554 1.6779 1.6934 1.7064 1.7168 1.7186 1.7186 1.7198 1.7195 1.7104 1.6991 1.6851 1.6636 1.6484
                                                   .
                                                   .
                                                   .

 ASSEMBLY NUMBER   86
 ASSEMBLY AVERAGE FUEL-ROD POWER BEFORE NORMALIZATION     .514
  1 1.4[illegible]7 1.4069 1.3382 1.2654 1.1928 1.1195 1.0406  .9626  .8861  .8102  .7308  .6491  .5597  .4494  .3009
  2 1.4851 1.4305 1.3837 1.2938 1.2224 1.1619 1.0687  .9807  .9116  .8443  .7534  .6693  .5852  .4642  .3098
  3 1.5001 1.4692  .0000 1.3392 1.2656  .0000 1.1169 1.0264  .9542  .0000  .7839  .6975  .0000  .4829  .3196
  4 1.5104 1.4626 1.4258 1.3532 1.2940 1.2156 1.1309  .0000  .9676  .8886  .8049  .7090  .6136  .4862  .3273
  5 1.5196 1.4744 1.4375 1.3806  .0000 1.2074 1.1095 1.0383  .9503  .8847  .0000  .7271  .6230  .4945  .3342
  6 1.5264 1.4995  .0000 1.3871 1.2915 1.1874 1.0940 1.0155  .9381  .8717  .8088  .7335  .0000  .5068  .3394
  7 1.5246 1.4812 1.4573 1.3853 1.2738 1.1743 1.1037 1.0371  .9470  .8635  .7997  .7353  .6380  .5037  .3419
  8 1.5229 1.4672 1.4447  .0000 1.2855 1.1751 1.1181  .0000  .9601  .8653  .8086  .0000  .6347  .5011  .3435
  9 1.5225 1.4803 1.4573 1.3865 1.2755 1.1765 1.1064 1.0402  .9705  .8672  .8034  .7392  .6417  .5070  .3443
 10 1.5221 1.4974  .0000 1.3890 1.2950 1.1920 1.0996 1.0218  .9449  .8791  .8164  .7413  .0000  .5134  .3443
 11 1.5134 1.4715 1.4377 1.3835  .0000 1.2146 1.1181 1.0480  .9606  .8958  .0000  .7384  .6337  .5041  .3410
 12 1.5023 1.4589 1.4262 1.3573 1.3014 1.2253 1.1426  .0000  .9817  .9032  .8199  .7238  .6276  .4982  .3363
 13 1.4900 1.4643  .0000 1.3442 1.2744  .0000 1.1313 1.0424  .9715  .0000  .8020  .7156  .0000  .4980  .3303
 14 1.4727 1.4246 1.3839 1.2995 1.2325 1.1759 1.0850  .9990  .9314  .8653  .7746  .6901  .6057  .4819  .3227
 15 1.4630 1.3991 1.3378 1.2711 1.2037 1.1348 1.0593  .9836  .9089  .8343  .7555  .6758  .5835  .4708  .3170
EOF
```

**Legend**:
For eight core burnup steps the assembly pin powers are given for each assembly in the top right quadrant of the core. For each assembly an array of 15 x 15 relative pin powers p(i,j) is given. The assembly is oriented as in Fig. 1.5; pin(1,1) is in the top left corner, pin(1,15) in the top right corner, pin(15,1) in the bottom left corner and pin(15,15) in the bottom right corner.

For each assembly in the top right quadrant of the core the following is given:

ASSEMBLY NUMBER    #..........assembly number as in Fig. 1.5; one record.
**Format**: (' ASSEMBLY NUMBER   ',I3)

ASSEMBLY AVERAGE FUEL-ROD POWER BEFORE NORMALIZATION.... assembly average fuel-rod power is equal to the relative assembly power.
**Format**: (' ASSEMBLY AVERAGE FUEL-ROD POWER BEFORE NORMALIZATION    ',F5.3)

Row number i, pin powers  p(i,j),j=1,15; fifteen records. Pin powers are normalized so that the average of the fuel-pin powers (204 per assembly) is 1.000.
**Format**: (I3,15F7.4).

**Fig. 1.11 Content and format of the FILE6.DAT.** Beginning and end of file are shown

```
  C0147MWd/MT
  1    .04662     .07495     .08855     .09196     .09584     .09618
       .09872     .09612     .09394     .08788     .07724     .05199
  2    .04607     .07432     .08827     .09209     .09602     .09636
       .09891     .09631     .09413     .08805     .07739     .05208
                                     .
                                     .
                                     .
156    .05030     .07704     .08863     .09508     .09722     .09821
       .09986     .09596     .09400     .08686     .07278     .04404
157    .03839     .06957     .08568     .09152     .09607     .09696
       .09859     .09707     .09587     .09165     .08082     .05780
                                     .
                                     .
                                     .
  10379MWd/MT
  1    .07266     .09436     .09279     .08585     .08551     .08275
       .08349     .08130     .08161     .08257     .08181     .07530
  2    .07118     .09300     .09242     .08613     .08589     .08312
       .08386     .08166     .08197     .08295     .08218     .07564
                                     .
                                     .
                                     .
157    .05238     .08230     .09055     .08942     .08940     .08700
       .08669     .08578     .08371     .08479     .08520     .08278
EOF
```

**Legend:**
For eight core burnup steps, the following is given.

Ass. # ........assembly number as in Fig. 1.5.
Relative powers of the axial segments of the assembly. There are 12 segments per assembly and each segment is 30.48 cm long (1 ft). The first segment (after Ass. #) is at the top of the active fuel and the last segment is at the bottom of the fuel. Normalization is to the sum of the segment powers equal to 1.00 in any assembly.

**Format:** (I3,6F10.5/3X,6F10.5)

**Fig. 1.12 Content and format of the FILE7.DAT.** Beginning and end of file are shown

```
YYMMDD        BU        LF        DTG Temp.
           MWd/MTU       %        MWd 100°F
820801        .0        .0         .0 5.250
820802        .0        .0         .0  .000
820803        .0        .0         .0  .000
820804        .0        .0         .0 4.080
820805        .0        .0         .0 5.300
820806        .0        .0         .0 3.440

                         .
                         .
                         .

840126 10636.8      34.0      782.2 5.354
840127 10636.8        .0         .0 5.030
840128 10636.8        .0         .0  .000
840129 10636.8        .0         .0  .000
840130 10636.8        .0         .0 1.2[illegible]
840131 10636.8        .0         .0 1.170
EOF
```

**Legend:**

```
YYMMDD...year,month,day.
BU.......core average cycle burnup
         in MWd/MTU.
LF.......load factor in percents;
         LF=100*(daily average
         power/2300MW).
DTG......daily thermal generation in MWd.
Temp.....core average coolant temperature
         in 100°F.(e.g., 5.354 is 535.4°F).
```

**Format:** (X,3I2,F8.1,F7.1,F8.1,F6.3)

**Fig. 1.13 Content and format of the FILE8.DAT.** Beginning and end of file are shown

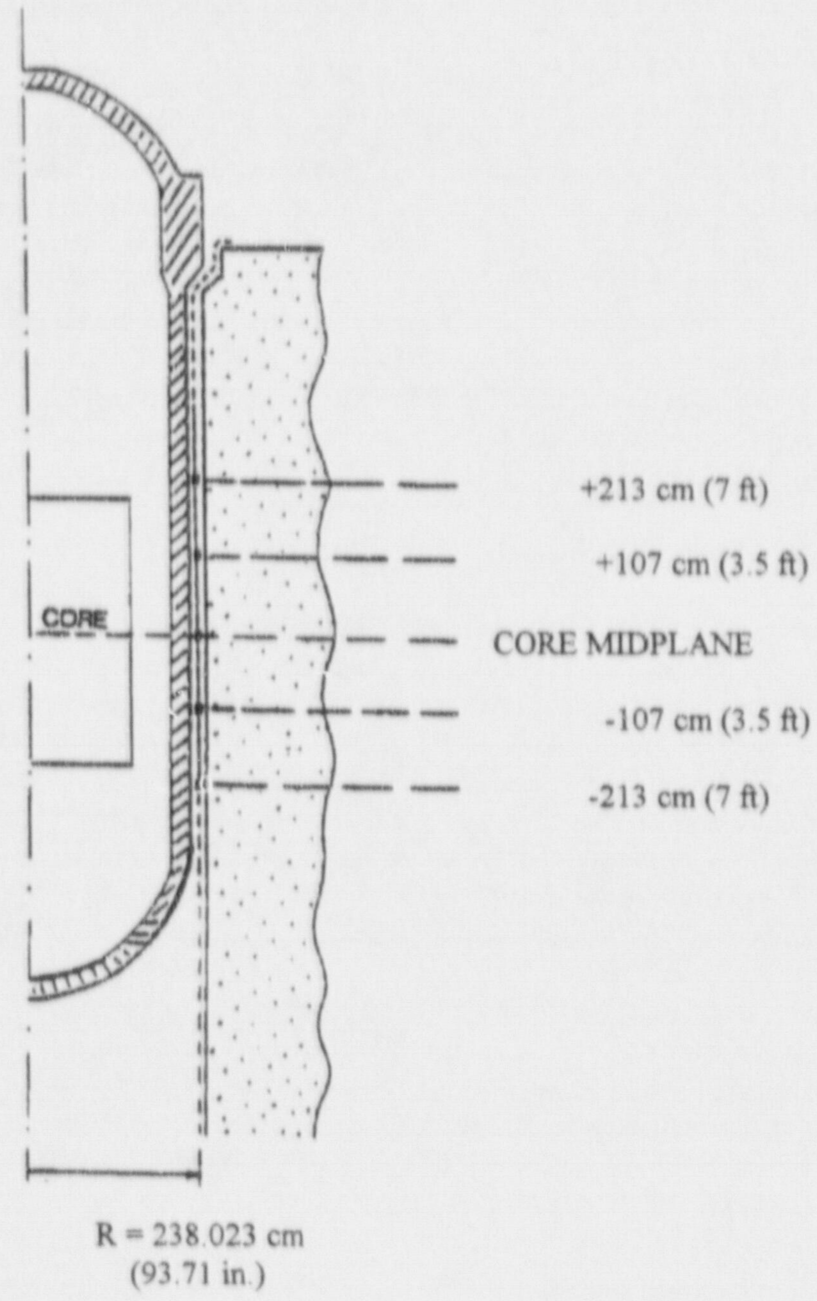


**Fig. 1.14 Schematic drawing of the axial positions of the cavity dosimeters.** At each of the marked locations a multiple dosimeter set was irradiated. Data in Table 1.4 are for the set in the core midplane

# 2 BENCHMARK ANALYSIS

## 2.1 METHODOLOGY

This section describes the analysis of the HBR-2 benchmark. The transport calculations were performed using the DORT computer code (Ref. 1) and the flux synthesis method.* The synthesis method, described in more detail in Ref. 2, relies on two- and one-dimensional (2-D and 1-D) transport calculations to obtain an estimation of the neutron fluxes in the three-dimensional (3-D) geometries. When the method is used to analyze a neutron field in a region outside the core of a pressurized water reactor, it calls for three transport calculations. One 2-D calculation models the horizontal cross section of the reactor in the $r$ - $\theta$ geometry. It is used to compute the variations of the neutron field in the radial direction (which is the main direction of the neutron transport from the core toward the pressure vessel and beyond) and in the azimuthal direction. The second calculation is a 2-D calculation in cylindrical $r$ - $z$ geometry, in which a core is modeled as a finite-height cylinder. The third calculation is made for the 1-D ($r$) cylindrical model of the reactor. The $r$ - $z$ and 1-D $r$- calculations are combined to obtain the axial variations of the neutron field.

Geometry models used in this analysis were almost identical to those used in the previous HBR-2 analysis (Refs. 2, 3). The $r$ - $\theta$ model covered one octant of the horizontal cross section with 74 azimuthal ($\theta$) intervals. In the radial direction—which extended from the core axis to the pressure vessel, the reactor cavity and inside the concrete shield (from a radius of 0 to 345 cm)—the number of radial intervals was varied with azimuthal interval (variable mesh option) and ranged from 93 to 116 intervals. The surveillance capsule was included in the model. The $r$ - $z$ model used 75 axial ($z$-axis) intervals (57 intervals covered the active fuel height of 365.76 cm) and 93 radial intervals (from the axis of the core to the radius of 335 cm). The $r$ - $z$ mesh outside the core described the geometry at the azimuth of 0°, since the benchmark cavity dosimetry is at the 0° azimuth. The one-dimensional calculation used the same radial mesh as the $r$ - $z$ model.

For the transport calculations, the cross sections of the macroscopic mixtures were prepared by the GIP code (Ref. 4), using the homogenized zone compositions given in Table 1.2 of this report. The $P_3$ approximation to the angular dependence of the anisotropic scattering cross sections (i.e., the $P_0$ to $P_3$ Legendre components) were taken into account, and a symmetric $S_8$ "directional quadrature set" (i.e., a set of discrete directions and angular quadratures) were used for all transport calculations. The benchmark was analyzed with three cross-section libraries based on ENDF/B-VI: BUGLE-93 (Ref. 5), SAILOR-95,† and BUGLE-96 (Ref. 6), which have 47 neutron and 20 gamma energy groups.

---

*DORT version 2.12.14, dated December 14, 1994, was used.

†Regarding SAILOR-95, see M. L. Williams, M. Asgari, and H. Manohara, "Letter Report on Generating SAILOR-95 Library," personal communication to F. B. K. Kam, ORNL, February 1995.

The neutron sources for the $r$ - $\theta$, $r$ - $z$ and one-dimensional calculation were prepared by the DOTSOR code.‡ For the $r$ - $\theta$ source, the cycle-averaged pin-power distributions in $x$ - $y$ geometry and cycle-average assembly powers were input into the DOTSOR, which transformed the power distribution into the $r$ - $\theta$ geometry mesh. The power-to-neutron-source conversion factor was based on the average burnup of the peripheral assemblies (i.e., assemblies 71, 86, and 101) at the middle of cycle 9, in order to account for the contributions of $^{235}$U and $^{239}$Pu to the fission neutron source.** The source energy spectrum was taken as the average of $^{235}$U and $^{239}$Pu fission spectra.††

The source for the $r$ - $z$ calculation was generated by averaging the cycle-average pin powers of the top halves of the fuel elements 79 to 86 over the $y$ axis (see Fig. 1.1; the y axis is perpendicular to the 0° radial direction) and multiplying the average pin-power values by the cycle-average axial power distribution of the corresponding fuel assembly. The $x$ - $z$ power distribution obtained was then transformed into $r$ - $z$ mesh by the DOTSOR code, which also prepared the source for 1-D $r$ calculation by integrating the $r$ - $z$ source over the $z$ axis. The same source energy spectrum as in the $r$ - $\theta$ calculation was used for the $r$ - $z$ and $r$ calculations.

From the three transport calculations, the neutron fluxes in the core midplane, in the surveillance capsule at the azimuth of 20°, and in the cavity at the azimuth of 0° were synthesized. Reaction rates were calculated with the CROSS-95 dosimetry library (Ref. 7). The CROSS-95 cross sections were collapsed from the 640 to 47 energy groups using the FLXPRO code from the LSL-M2 code package (Ref. 8) and the reference spectra as calculated in the capsule and cavity location. The reaction rates are listed in Table 2.1.

To calculate the specific activities at the end of irradiation, which are the measured quantities provided for comparison with the calculations, it is necessary to take into account the reactor power changes during irradiation and other changes that may affect the reaction rates. As a result of fuel burnup the power distribution in the core changes gradually throughout the fuel cycle, causing changes in neutron leakage from the core and consequent changes in reaction rates at the dosimetry locations. Since the reaction rates were calculated for one power distribution only (i.e., the cycle-average power distribution) approximations are necessary to account for these gradual changes.

---

‡Regarding DOTSOR, see M. L. Williams, *DOTSOR: A Module in the LEPRICON Computer Code System for Representing the Neutron Source Distribution in LWR Cores*, EPRI Research Project 1399-1 Interim Report (December 1985), RSIC Peripheral Shielding Routine Collection PSR-277.

**The power-to-neutron-source conversion factor of $8.175 \times 10^{16}$ neutrons $s^{-1}MW^{-1}$ was calculated by the DOTSOR code for the fuel burnup of 28596 MWd/MTU, which corresponds to the cycle-average burnup of the fuel assemblies number 71, 86, and 101.

††The ENDF/B-VI fission spectra for $^{235}$U and $^{239}$Pu were used.

Reaction rates at the dosimetry location are affected mostly by the closest fuel assemblies. Therefore, for the cavity-dosimetry location, the following approximation was used. The cycle was divided into eight time intervals, based on the burnup steps at which the power distributions were provided. That is, the first interval was taken from the beginning of cycle to the core burnup halfway between the first and second power distribution provided, the second interval from the end of the first interval to halfway between the second and third power distribution, etc. The average relative power $p_i$ of the three fuel elements on the core flat edge (i.e., assemblies 71, 86, and 101) was calculated and assumed constant during the corresponding interval. The average relative powers ($p_i$) were normalized so that, when integrated over the cycle, they provide the correct total energy produced (i.e., the average energy produced in the three fuel elements, as given in FILE1.DAT). Using the daily power history, the reaction rate was then approximated as

$$R_j = R_c \times (p_i / p_{DORT}) \times (P_j / P_o), \tag{2.1}$$

where

- $R_j$ = reaction rate at cavity location during $j$-th day,
- $R_c$ = reaction rate obtained from transport (DORT) calculations, for nominal core power,
- $p_i$ = normalized average relative power of the fuel elements 71, 86, and 101 during $i$-th time interval,
- $p_{DORT}$ = average relative power of the fuel elements 71, 86, and 101 used in the transport calculation (DORT),
- $P_j$ = daily-average reactor core power during day $j$. (Day $j$ is in the time interval $i$).
- $P_o$ = nominal core power (2300 MW).

The same procedure was used for the calculation of activities of the dosimeters in the surveillance capsule; however, the fuel assemblies considered were the ones closest to the capsule location— that is, assemblies 43, 56, and 71.

Different approaches can be used to account for the changes of reaction rates during the cycle; for example, one can (1) simply neglect the effects of redistribution and account only for the core power variations or (2) use the adjoint scaling techniques described in Ref. 2. The impact of different approaches on the calculated specific activities is further discussed in Appendix A.

## 2.2 RESULTS AND DISCUSSION

The reaction rates calculated as described in the previous subsection, for the cycle-average power distribution, are given in Table 2.1. The reaction rates obtained from the transport calculations with the BUGLE-93, SAILOR-95, and BUGLE-96 are practically identical in the surveillance capsule, for all the reactions considered; the maximum differences are less than 1%. In the cavity the reaction rates obtained by BUGLE-96 and SAILOR-95 agree to better than 1%. The reaction rates obtained by BUGLE-93 for the $^{63}$Cu($n,\alpha$) and $^{46}$Ti($n,p$) reactions are practically identical to those obtained by the other two libraries, while BUGLE-93 reaction rates for $^{54}$Fe($n,p$), $^{58}$Ni($n,p$), $^{238}$U($n,f$), and $^{237}$Np($n,f$) are 1%, 2%, 4% and 10% lower, respectively, than reaction rates calculated with the other two libraries. These observations are consistent with the results of the Pool Critical Assembly Pressure Vessel Facility Benchmark analysis, where good agreement of the reaction rates obtained by all three libraries was found for the dosimeters located inside the pressure vessel, while in the void box behind the pressure vessel (simulating the reactor cavity), the BUGLE-93 predicted lower reaction rates than the other two libraries, for all the dosimeters except $^{237}$Np, for which the BUGLE-93 predicted a higher reaction rate (Ref. 9).

**Table 2.1 Reaction rates calculated for the cycle-average power distribution and core power of 2300 MW (100% of nominal power), with different cross-section libraries for transport calculations**

| Cross-Section Library | Reaction Rate ($s^{-1}$ $atom^{-1}$) | | | | | |
|---|---|---|---|---|---|---|
| | $^{237}$Np($n,f$) | $^{238}$U($n,f$) | $^{58}$Ni($n,p$) | $^{54}$Fe($n,p$) | $^{46}$Ti($n,p$) | $^{63}$Cu($n,\alpha$) |
| | **Capsule** | | | | | |
| BUGLE-93 | 1.05E-13 | 1.54E-14 | 4.74E-15 | 3.50E-15 | 5.62E-16 | 3.57E-17 |
| SAILOR-95 | 1.06E-13 | 1.55E-14 | 4.77E-15 | 3.52E-15 | 5.64E-16 | 3.58E-17 |
| BUGLE-96 | 1.06E-13 | 1.54E-14 | 4.74E-15 | 3.51E-15 | 5.62E-16 | 3.57E-17 |
| | **Cavity** | | | | | |
| BUGLE-93 | 3.72E-15 | 2.04E-16 | 4.72E-17 | 3.20E-17 | 5.16E-18 | 3.63E-19 |
| SAILOR-95 | 4.14E-15 | 2.12E-16 | 4.82E-17 | 3.24E-17 | 5.18E-18 | 3.64E-19 |
| BUGLE-96 | 4.13E-15 | 2.11E-16 | 4.79E-17 | 3.23E-17 | 5.16E-18 | 3.63E-19 |

With the reaction rates from Table 2.1 the specific activities were calculated as described in subsection 2.1. The calculated specific activities are given in Table 2.2. Conversion from reaction rates to specific activities does not affect the differences between results obtained by different cross-section libraries; therefore, for the comparison of specific activities the comments given above for the reaction rates apply.

**Table 2.2 Calculated specific activities**

| Cross-Section Library | Specific activity (Bq/mg) | | | | | |
|---|---|---|---|---|---|---|
| | $^{237}Np(n,f)$ $^{137}Cs$ | $^{238}U(n,f)$ $^{137}Cs$ | $^{58}Ni(n,p)$ $^{58}Co$ | $^{54}Fe(n,p)$ $^{54}Mn$ | $^{46}Ti(n,p)$ $^{46}Sc$ | $^{63}Cu(n,\alpha)$ $^{60}Co$ |
| $T_{1/2}$* | 30 years | 30 years | 71 days | 313 days | 84 days | 5.3 years |
| **Capsule** | | | | | | |
| BUGLE-93 | 3.28E+2 | 4.52E+1 | 1.70E+4 | 8.68E+2 | 2.96E+2 | 2.39E+1 |
| SAILOR-95 | 3.31E+2 | 4.56E+1 | 1.71E+4 | 8.73E+2 | 2.98E+2 | 2.40E+1 |
| BUGLE-96 | 3.30E+2 | 4.54E+1 | 1.71E+4 | 8.69E+2 | 2.96E+2 | 2.39E+1 |
| **Cavity** | | | | | | |
| BUGLE-93 | 1.17E+1 | 6.06E-1 | 1.88E+2 | 8.27 | 2.99 | 2.47E-1 |
| SAILOR-95 | 1.30E+1 | 6.30E-1 | 1.91E+2 | 8.36 | 3.00 | 2.47E-1 |
| BUGLE-96 | 1.30E+1 | 6.28E-1 | 1.91E+2 | 8.32 | 2.99 | 2.47E-1 |

* Reaction product half-life.

Table 2.3 lists the ratios of the calculated and measured specific activities. Calculated specific activities are taken from Table 2.2. Measured specific activities are taken from Table 1.4. The average C/M ratios in the capsule, for BUGLE-93, SAILOR-95, and BUGLE-96, are 0.90 ± 0.04, 0.90 ± 0.04, and 0.90 ± 0.04, respectively. If the corrections, discussed in notes to Table 1.4, are applied to the measured activities of the $^{237}Np$, $^{238}U$, and $^{63}Cu$ dosimeters, the C/M ratios increase by ~3%, 6%, and 3% in the capsule, respectively, and by ~6%, 11%, and 3% in the cavity, respectively. The C/M ratios for the corrected measured activities are listed in Table 2.3 in parentheses.

**Table 2.3 Ratios of calculated-to-measured (C/M) specific activities***

| Cross-Section Library | $^{237}Np(n,f)$ $^{137}Cs$ | $^{238}U(n,f)$ $^{137}Cs$ | $^{58}Ni(n,p)$ $^{58}Co$ | $^{54}Fe(n,p)$ $^{54}Mn$ | $^{46}Ti(n,p)$ $^{46}Sc$ | $^{63}Cu(n,\alpha)$ $^{60}Co$ | Average† |
|---|---|---|---|---|---|---|---|
| $T_{1/2}$‡ | 30 years | 30 years | 71 days | 313 days | 84 days | 5.3 years | |
| **Capsule** | | | | | | | |
| BUGLE-93 | 0.89 (0.92) | 0.85 (0.89) | 0.95 | 0.93 | 0.85 | 0.90 (0.93) | 0.90 ± 0.04 (0.91 ± 0.04) |
| SAILOR-95 | 0.90 (0.92) | 0.85 (0.90) | 0.96 | 0.93 | 0.85 | 0.91 (0.93) | 0.90 ± 0.04 (0.92 ± 0.04) |
| BUGLE-96 | 0.90 (0.92) | 0.85 (0.89) | 0.96 | 0.93 | 0.85 | 0.90 (0.93) | 0.90 ± 0.04 (0.91 ± 0.04) |
| **Cavity** | | | | | | | |
| BUGLE-93 | 0.52 (0.55) | 0.71 (0.79) | 0.96 | 0.95 | 0.90 | 0.93 (0.96) | 0.89 ± 0.10 (0.91 ± 0.07) |
| SAILOR-95 | 0.58 (0.61) | 0.74 (0.82) | 0.98 | 0.96 | 0.91 | 0.94 (0.96) | 0.91 ± 0.10 (0.93 ± 0.06) |
| BUGLE-96 | 0.58 (0.61) | 0.74 (0.82) | 0.97 | 0.96 | 0.90 | 0.93 (0.96) | 0.90 ± 0.09 (0.92 ± 0.06) |

* Ratios C/M are given for the as-measured specific activities. The ratios given in parentheses are calculated with corrections, specified in Table 1.4, applied to $^{237}Np(n,f)^{137}Cs$, $^{238}U(n,f)^{137}Cs$, and $^{63}Cu(n,\alpha)^{60}Co$ measured reaction rates.

† Average C/M ratio and standard deviation. For the cavity location averages are calculated without $^{237}Np(n,f)^{137}Cs$ reaction. The averages with $^{237}Np(n,f)^{137}Cs$ reaction are 0.83 ± 0.18 (0.85 ± 0.16), 0.85 ± 0.16 (0.87 ± 0.14), and 0.85 ± 0.16 (0.87 ± 0.14), for BUGLE-93, SAILOR-95, and BUGLE-96 libraries, respectively. Values in parentheses are calculated with corrections applied to $^{237}Np$, $^{238}U$, and $^{63}Cu$ dosimeters, as discussed in the footnote above.

‡ Reaction product half-life.

In the cavity the C/M ratio for the $^{237}Np$ dosimeter is significantly lower than C/M ratios for other dosimeters, regardless of the cross-section library used.* Therefore, the average C/M values in the cavity, given in Table 2.3 in the last column on the right, were calculated without the Np dosimeter.

---

*This well-known problem of the HBR-2 cycle 9 cavity dosimetry measurements was addressed in several analyses, but has not been completely explained. Currently the most probable explanation appears to be an incorrect measured value.

The average C/M values in the cavity for BUGLE-93, SAILOR-95, and BUGLE-96 are 0.89 ± 0.10, 0.91 ± 0.10, and 0.90 ± 0.09, respectively.† The C/M ratios given in parentheses are for the measured activities of $^{237}$Np, $^{238}$U, and $^{63}$Cu dosimeters, corrected as discussed in notes to Table 1.4. The average C/M ratios in the cavity are practically identical to those in the capsule; therefore, no decrease in the C/M ratios with increasing distance from the core and increasing thickness of steel penetrated is observed. Such decrease was typical for the pre-ENDF/B-VI cross-section libraries and is illustrated in Appendix A.

The variations of the C/M values for different dosimeters at the same location are small: the standard deviation of the average C/M ratios is ~0.04 in the capsule and ~0.10 in the cavity.‡ These values suggest that the shapes of the calculated spectra, in the energy range to which the measured dosimeters are sensitive, are adequate. To further assess the differences between the three libraries the calculated multigroup neutron spectra are tabulated and compared in Appendix B. The tabulated spectra were used to determine the reaction rates given in Table 2.1. In the capsule the multigroup fluxes calculated with the BUGLE-93, SAILOR-95, and BUGLE-96 libraries agree to within ~2%, except at thermal energies where differences are bigger: below ~0.1eV SAILOR-95 and BUGLE-93 predicted, respectively, ~2 times lower and 2.7 times higher flux than BUGLE-96 (see Fig. B.2). These differences at the low energies are not important for predicting radiation damage in the steel specimens and reaction rates of the threshold neutron dosimeters in the capsule.

In the cavity, the group fluxes calculated with the SAILOR-95 and BUGLE-96 libraries agree to better than 1% over the entire energy range while the BUGLE-93 fluxes differ considerably (see Fig. B.4). BUGLE-93 predicted up to two times higher fluxes below 1eV, and, more importantly, lower fluxes at higher energies, except between ~10keV and 70keV. Between ~0.1MeV and 2MeV, BUGLE-93 predicted at least 5% lower fluxes than BUGLE-96, with the maximum difference about 18% at ~0.7 MeV. This comparison, combined with the observation that the calculations underpredicted the reaction rates, suggests that neutron flux and spectrum in the cavity are more accurately predicted by the BUGLE-96 library than by the BUGLE-93 library. Some support for this suggestion can also be found from the comparison of the calculated and measured specific activities (see Table 2.3). In the cavity, the BUGLE-93 library gave slightly lower C/M ratios than the other two libraries for the $^{58}$Ni dosimeter and in particular for the $^{238}$U and $^{237}$Np dosimeters, which have lower reaction energy thresholds and are sensitive to the neutrons below ~2MeV. Similar differences, as observed here between the multigroup fluxes calculated by the BUGLE-93 and BUGLE-96 libraries, were also found in the analysis of the Pool Critical Assembly Pressure Vessel Facility (Ref. 9).

---

†If the $^{237}$Np dosimeter in the cavity is taken into account, the average C/M values are 0.83 ± 0.18, 0.85 ± 0.16, and 0.85 ± 0.16, for the BUGLE-93, SAILOR-95, and BUGLE-96 library, respectively.

‡If the $^{237}$Np dosimeter in the cavity is taken into account, the standard deviation of the average C/M is ~0.16.

## 2.3 REFERENCES


1. W. A. Rhoades et al., "TORT-DORT Two- and Three-Dimensional Discrete Ordinates Transport, Version 2.8.14," CCC-543, Radiation Shielding Information Center, Oak Ridge National Laboratory, 1994.

2. R. E. Maerker, "LEPRICON Analysis of the Pressure Vessel Surveillance Dosimetry Inserted into H. B. Robinson-2 During Cycle 9," *Nuc. Sci. Eng.*, 96:263 (1987).

3. M. L. Williams, M. Asgari, F. B. K. Kam, *Impact of ENDF/B-VI Cross-Section Data on H. B. Robinson Cycle 9 Dosimetry Calculations*, NUREG/CR-6071 (ORNL/TM-12406), October 1993.

4. W. A. Rhoades,"The GIP Program for Preparation of Group-Organized Cross-Section Libraries," informal notes, November 1975, RSIC Peripheral Shielding Routine Collection PSR-75.

5. D. T. Ingersoll et al.,"Bugle-93: Coupled 47 Neutron, 20 Gamma-Ray Group Cross-Section Library Derived from ENDF/B-VI for LWR Shielding and Pressure Vessel Dosimetry Applications," RSIC Data Library Collection, DLC-175, February 1994.

6. J. E. White et al.,"BUGLE-96: Coupled 47 Neutron, 20 Gamma-Ray Group Cross Section Library Derived from ENDF/B-VI for LWR Shielding and Pressure Vessel Dosimetry Applications," RSIC Data Library Collection, DLC-185, March 1996.

7. I. Remec and F. B. K. Kam, *An Update of the Dosimetry Cross-Section Data Base for the Adjustment Code LSL-M2*, ORNL/NRC/LTR-95/20, June 1995.

8. F. W. Stallmann, *LSL-M2: A Computer Program for Least-Squares Logarithmic Adjustment of Neutron Spectra*, NUREG/CR-4349 (ORNL/TM-9933), March 1986.

9. I. Remec and F. B. K. Kam, *Pool Critical Assembly Pressure Vessel Facility Benchmark*, NUREG/CR-6454 (ORNL/TM-13205), July 1997.

# 3 CONCLUSIONS

Section 1 of this report describes the HBR-2 pressure vessel dosimetry benchmark and provides all the dimensions, material compositions and neutron source data necessary for the analysis. The neutron source data are provided on the floppy disk accompanying this report.

In Section 2, the analysis of the HBR-2 benchmark is presented. The transport calculations with the computer code DORT, based on the discrete-ordinates method, were performed with three ENDF/B-VI-based multigroup libraries: BUGLE-93, SAILOR-95, and BUGLE-96. Excellent agreement of the calculated specific activities with the measurements was obtained. For the dosimeters in the surveillance capsule, the average C/M ratios for BUGLE-93, SAILOR-95, and BUGLE-96, are $0.90 \pm 0.04$, $0.90 \pm 0.04$, and $0.90 \pm 0.04$, respectively. For the dosimeters irradiated in the cavity, the average C/M ratios (excluding $^{237}$Np dosimeter) for BUGLE-93, SAILOR-95, and BUGLE-96, are $0.89 \pm 0.10$, $0.91 \pm 0.10$, and $0.90 \pm 0.09$, respectively. The C/M ratios given above are for the as-measured specific activities (e.g., no corrections were applied to the $^{237}$Np, $^{238}$U, and $^{63}$Cu dosimeters). No systematic decrease in the C/M ratios with increasing distance from the core was observed for any of the libraries used.

It is expected that the agreements of the calculations with the measurements, similar to those shown in this report, should typically be obtained when the discrete-ordinates method and the ENDF/B-VI cross-section libraries are used for the HBR-2 benchmark analysis.

# APPENDIX A

## COMPARISON OF APPROXIMATIONS FOR MODELING THE REACTION RATE VARIATIONS DUE TO CORE POWER REDISTRIBUTION AND COMPARISON OF RESULTS OBTAINED WITH ENDF/B-IV AND ENDF/B-VI CROSS SECTIONS

In the steady-state neutron field the activities of the dosimeters during irradiation gradually approach the saturated activities, which are proportional to the reaction rates. For a given dosimeter and reaction rate, the activity of the dosimeter depends only on the time of irradiation. The transformation of the measured specific activity into the reaction rate is simple; it does not involve approximations and it does not introduce uncertainties other than those related to the characteristics of the dosimeter and reaction product. Therefore, the reaction rates deduced from activities measured in a steady-state neutron field are usually referred to as "measured" reaction rates.

However, in a power reactor the neutron field and consequently the reaction rates vary with time because (1) the power distribution in the core gradually changes with fuel burnup ("power-redistribution") and (2) the changes of the reactor power. The reaction rates are often calculated for a given core condition only (e.g., nominal thermal power, at certain core burnup), and approximations are necessary in the calculation of specific activities. To approximate the effect of the changes of the core power it is usually assumed that the reaction rates are proportional to the core power (at all locations of the dosimeters ). The changes in reaction rates caused by the power redistribution may vary from negligible to ~30 to 40%. These changes depend primarily on the fuel loading pattern (and, therefore, vary from cycle to cycle) and may be different for different dosimetry locations. Since the treatment of the power-redistribution effect is less standardized, the effect of a few different approximations is illustrated on the example of HBR-2 cycle 9 dosimetry analysis. The following approaches were considered:

(a) Changes due to redistribution were approximately accounted for as described insubsection 2.1 [e.g., the reaction rates were taken proportional to the core power (daily-averaged) and average relative power of the fuel assemblies closest to the location of the dosimeters].

(b) The redistribution effect was neglected, and reaction rates were taken proportional to the core power (daily-averaged).

(c) Reaction rates from the present analysis were converted into the specific activities by the conversion factors determined from Ref. 1. In Ref. 1 the adjoint scaling technique was used to determine the reaction rates for eight core power distributions during the cycle and then the specific activities were calculated by superimposing the power history. This method should be more accurate than the two approaches described above. However, in Ref. 1 the core power distributions from an older analysis were used, which may affect the reaction-rate-to-activity conversion factors and consequently the comparison with the results from steps (a) and (b).

Using the reaction rates obtained from the transport calculation with the BUGLE-96 library, the specific activities were calculated according to the three approximations described above. The C/M ratios for the capsule and cavity dosimeters are listed in Table A.1. In the capsule the three approximations give very similar average C/M ratios and corresponding standard deviations. This similarity exists because the changes of the power of the peripheral fuel assemblies closest to the capsule are relatively small; the average power of the elements number 43, 56, and 71 increased only ~20% from the beginning to the end of cycle. However, the average power of the assemblies on the flat edge (i.e., assemblies 71, 86 and 101) increased over 60% from the beginning to the end of the cycle, and this power increase affects the comparisons in the cavity. Approximations (a), (b), and (c) gave the average C/M values in the cavity of 0.90 ± 0.09, 0.83 ± 0.08, and 0.84 ± 0.08, respectively. The advantage of approximation (a) over (b) is clearly shown. The largest differences in the C/M ratios are observed for the reactions with short-lived products, $^{58}Ni(n,p)^{58}Co$ and $^{46}Ti(n,p)^{46}Sc$; the C/M for the fission dosimeters, for which the activity of long-lived $^{137}Cs$ is measured, are almost unaffected. The approximations (b) and (c) give very similar results: average C/M and its standard deviation in the cavity are 0.83 ± 0.08, and 0.84 ± 0.08, respectively, and in the capsule are 0.88 ± 0.04, and 0.89 ± 0.05, respectively. Therefore, in this case it appears that using the adjoint scaling technique [i.e., approximation (c)] gives little advantage over the simpler approximation (b),which accounts for core power variations only. However, the application of conversion factors, calculated from results obtained by adjoint scaling in Ref. 1, to the reaction rates calculated in the present analysis, is approximate, as described above.

The HBR-2 cycle 9 dosimetry has been analyzed before; see for example Refs. 1 and 2. In Ref. 1, ELXSIR cross sections (Ref. 3) based on ENDF/B-IV were used. In Ref. 2, SAILOR cross sections (Ref. 4) based on ENDF/B-IV with iron, oxygen, and hydrogen cross sections from the ENDF/B-VI library and ENDF/B-VI dosimetry cross sections were used. To assess the impact of the ENDF/B-VI-based cross-section library for transport calculations, the analysis was repeated with exactly the same neutron source (i. e., spatial power distribution in the core, and source energy spectrum between $^{235}U$ and $^{239}Pu$ ENDF/B-V fission spectra) and modeling approximations that were used in Refs. 1 and 2. For consistency (with Refs. 1 and 2), the time-dependent variations of reaction rates were approximated by using the mid-cycle reaction rates to the end-of-cycle activities conversion factors from Ref. 1, and the measured reaction rates were corrected as described in the note to Table 1.4. The SAILOR-95 (ENDF/B-VI-based) cross sections for transport calculations were used, and dosimetry cross sections were taken from CROSS-95. This analysis will be referred to in the following discussion as the "new" analysis. The C/M ratios for the capsule and cavity dosimeters from the new analysis are compared with the values from Refs. 1 and 2 in Table A.2.

In the capsule, the new analysis gave the average C/M of 0.93 ± 0.05, slightly lower than the average of 0.96 ± 0.05 from Ref. 2. This lower value is present probably because in the new analysis and in Ref. 2 the reaction rates inside the capsule were determined at slightly different radial locations. Both Ref. 2 and the new analysis gave significantly improved C/M values over the values from Ref. 1: the increase in the average C/M in the capsule is ~12% for the new analysis and ~16% for the Ref. 2.

In the cavity location, the new analysis and Ref. 2 gave practically identical results, with the average C/M of 0.88 ± 0.14, while the C/M average for the Ref. 1 is 0.66 ± 0.04. Therefore, the increase in the average C/M ratio is ~33%. For the $^{237}Np(n,f)^{137}Cs$ reaction the C/M ratio in the new analysis and in Ref. 2 is about 0.61 and differs significantly from the C/M ratios for the other dosimeters, as can be seen from Table A.2. The average C/M for the cavity location calculated without the $^{237}Np(n,f)^{137}Cs$ reaction is 0.93 for the new analysis and Ref. 2, and 0.67 for Ref. 1; therefore, an improvement of 39% was obtained.

The ENDF/B-VI-based cross sections for transport calculations resulted in improved agreement of calculations and measurements, both in the capsule and in the cavity. The average C/M in the capsule, for the six dosimeters used, is ~0.93 ± 0.05; the ENDF/B-IV-based library gave 0.83 ± 0.03. In the cavity, the average (excluding $^{237}$Np dosimeter) is 0.93 ± 0.06, and 0.67 ± 0.03 for the ENDF/B-VI- and ENDF/B-IV-based libraries, respectively. Therefore, the ENDF/B-VI-based cross sections eliminated the decrease of the C/M ratios with increasing distance from the core and increasing thickness of the steel penetrated by neutrons.

**Table A.1 Ratios of calculated-to-measured (C/M) specific activities obtained with different approximations for the time-dependent variations of reaction rates***

| | $^{237}Np(n,f)$ $^{137}Cs$ | $^{238}U(n,f)$ $^{137}Cs$ | $^{58}Ni(n,p)$ $^{58}Co$ | $^{54}Fe(n,p)$ $^{54}Mn$ | $^{46}Ti(n,p)$ $^{46}Sc$ | $^{63}Cu(n,\alpha)$ $^{60}Co$ | Average† |
|---|---|---|---|---|---|---|---|
| $T_{1/2}$‡ | 30 years | 30 years | 71 days | 313 days | 84 days | 5.3 years | |
| **Capsule** | | | | | | | |
| Approx. (a)** | 0.90 (0.92) | 0.85 (0.89) | 0.96 | 0.93 | 0.85 | 0.90 (0.93) | 0.90 ± 0.04 (0.91 ± 0.04) |
| Approx. (b)** | 0.90 (0.92) | 0.85 (0.89) | 0.90 | 0.91 | 0.80 | 0.90 (0.92) | 0.88 ± 0.04 (0.89 ± 0.05) |
| Approx. (c)** | 0.86 (0.88) | 0.82 (0.86) | 0.98 | 0.91 | 0.87 | 0.87 (0.89) | 0.89 ± 0.05 (0.90 ± 0.04) |
| **Cavity** | | | | | | | |
| Approx. (a)** | 0.58 (0.61) | 0.74 (0.82) | 0.97 | 0.96 | 0.90 | 0.93 (0.96) | 0.90 ± 0.09 (0.92 ± 0.06) |
| Approx. (b)** | 0.57 (0.60) | 0.73 (0.80) | 0.83 | 0.90 | 0.78 | 0.92 (0.94) | 0.83 ± 0.08 (0.85 ± 0.07) |
| Approx. (c)** | 0.55 (0.57) | 0.70 (0.77) | 0.90 | 0.90 | 0.84 | 0.88 (0.91) | 0.84 ± 0.08 (0.86 ± 0.06) |

* Ratios C/M are given for the as-measured specific activities. The ratios given in parentheses are calculated with corrections, specified in Table 1.4, applied to $^{237}Np(n,f)^{137}Cs$, $^{238}U(n,f)^{137}Cs$, and $^{63}Cu(n,\alpha)^{60}Co$ measured reaction rates.

† Average C/M ratio and standard deviation. For the cavity location, averages are calculated without $^{237}Np(n,f)^{137}Cs$ reaction. The averages with $^{237}Np(n,f)^{137}Cs$ reaction are 0.85 ± 0.16 (0.87 ± 0.14), 0.79 ± 0.13 (0.81 ± 0.12), and 0.80 ± 0.14 (0.82 ± 0.13), for methods (a), (b), and (c), respectively. Values in parentheses are calculated with corrections applied to $^{237}Np$, $^{238}U$, and $^{63}Cu$ dosimeters, as discussed in the footnote above.

‡ Reaction product half-life.

** See text for the explanation of the approximations (a), (b), and (c).

**Table A.2 Comparison of the C/M ratios of specific activities from the present analysis with the values from the previous analyses (Refs. 1 and 2)**

| | C/M ratios | | | | | | |
|---|---|---|---|---|---|---|---|
| | $^{237}Np(n,f)$ $^{137}Cs$ | $^{238}U(n,f)$ $^{137}Cs$ | $^{58}Ni(n,p)$ $^{58}Co$ | $^{54}Fe(n,p)$ $^{54}Mn$ | $^{46}Ti(n,p)$ $^{46}Sc$ | $^{63}Cu(n,\alpha)$ $^{60}Co$ | Average C/M $\pm\sigma$ |
| **Capsule** | | | | | | | |
| New Analysis* | 0.91 | 0.89 | 1.01 | 0.95 | 0.89 | 0.91 | 0.93 ± 0.05 |
| Analysis from Ref. 1† | 0.85 | 0.80 | 0.87 | 0.83 | 0.81 | 0.83 | 0.83 ± 0.03 |
| Analysis from Ref. 2‡ | 0.94 | 0.93 | 1.05 | 0.98 | 0.92 | 0.95 | 0.96 ± 0.05 |
| **Cavity** | | | | | | | |
| New Analysis* | 0.62 | 0.84 | 0.98 | 0.97 | 0.89 | 0.95 | 0.88 ± 0.14 (0.93 ± 0.06)** |
| Analysis from Ref. 1† | 0.61 | 0.65 | 0.66 | 0.68 | 0.66 | 0.72 | 0.66 ± 0.04 (0.67 ±0.03)** |
| Analysis from Ref. 2‡ | 0.61 | 0.86 | 0.97 | 0.97 | 0.90 | 0.96 | 0.88 ± 0.14 (0.93 ± 0.05)** |

* New analysis, using SAILOR-95 and CROSS-95 cross sections.

† Results from Ref. 1, using ELXSIR cross sections, based on ENDF/B-IV.

‡ Results from Ref. 2, using SAILOR cross sections (based on ENDF/B-IV) with iron, oxygen, and hydrogen cross sections from ENDF/B-VI library and ENDF/B-VI dosimetry cross-sections.

** C/M for neptunium omitted from the average.

## APPENDIX A REFERENCES


1. R. E. Maerker, "LEPRICON Analysis of the Pressure Vessel Surveillance Dosimetry Inserted into H. B. Robinson-2 During Cycle 9," *Nuc. Sci. Eng.*, 96:263 (1987).

2. M. L. Williams, M. Asgari, F. B. K. Kam, *Impact of ENDF/B-VI Cross-Section Data on H. B. Robinson Cycle 9 Dosimetry Calculations*, NUREG/CR-6071 (ORNL/TM 12406), October 1993.

3. M. L. Williams et al., *The ELXSIR Cross-Section Library for LWR Pressure Vessel Irradiation Studies: Part of the LEPRICON Computer Code System*, EPRI NP-3654, Electric Power Research Institute, Palo Alto, Calif.,1984.

4. G. L. Simmons and R. W. Roussin, "SAILOR- Coupled, Self-Shielded, 47 Neutron, 20 Gamma-Ray, $P_3$, Cross-Section Library for Light Water Reactors," DLC-76, Radiation Shielding Information Center, Oak Ridge National Laboratory, 1985.

# APPENDIX B

# CALCULATED NEUTRON SPECTRA AT THE DOSIMETRY LOCATIONS

**Table B.1 Calculated multigroup neutron fluxes in the surveillance capsule** (20° azimuth, core midplane, at the radius of 191.15 cm from core vertical axis)

| Group number | Group upper energy limit | Neutron flux BUGLE-93 | Neutron flux SAILOR-95 | Neutron flux BUGLE-96 |
|---|---|---|---|---|
| | eV | $cm^{-2} s^{-1}$ | $cm^{-2} s^{-1}$ | $cm^{-2} s^{-1}$ |
| 1 | 1.733E+07 | 8.870E+06 | 8.870E+06 | 8.870E+06 |
| 2 | 1.419E+07 | 2.808E+07 | 2.808E+07 | 2.808E+07 |
| 3 | 1.221E+07 | 1.207E+08 | 1.207E+08 | 1.207E+08 |
| 4 | 1.000E+07 | 2.379E+08 | 2.379E+08 | 2.379E+08 |
| 5 | 8.607E+06 | 4.113E+08 | 4.117E+08 | 4.112E+08 |
| 6 | 7.408E+06 | 9.984E+08 | 1.001E+09 | 9.984E+08 |
| 7 | 6.065E+06 | 1.485E+09 | 1.493E+09 | 1.485E+09 |
| 8 | 4.966E+06 | 2.865E+09 | 2.891E+09 | 2.866E+09 |
| 9 | 3.679E+06 | 2.219E+09 | 2.229E+09 | 2.220E+09 |
| 10 | 3.012E+06 | 1.710E+09 | 1.719E+09 | 1.713E+09 |
| 11 | 2.725E+06 | 1.998E+09 | 2.005E+09 | 2.001E+09 |
| 12 | 2.466E+06 | 9.928E+08 | 9.989E+08 | 9.963E+08 |
| 13 | 2.365E+06 | 2.768E+08 | 2.786E+08 | 2.779E+08 |
| 14 | 2.346E+06 | 1.383E+09 | 1.392E+09 | 1.388E+09 |
| 15 | 2.231E+06 | 3.767E+09 | 3.790E+09 | 3.780E+09 |
| 16 | 1.920E+06 | 4.382E+09 | 4.427E+09 | 4.411E+09 |
| 17 | 1.653E+06 | 6.576E+09 | 6.664E+09 | 6.633E+09 |
| 18 | 1.353E+06 | 1.190E+10 | 1.207E+10 | 1.203E+10 |
| 19 | 1.003E+06 | 8.127E+09 | 8.258E+09 | 8.228E+09 |
| 20 | 8.208E+05 | 4.085E+09 | 4.147E+09 | 4.136E+09 |
| 21 | 7.427E+05 | 1.150E+10 | 1.180E+10 | 1.176E+10 |
| 22 | 6.081E+05 | 9.276E+09 | 9.333E+09 | 9.306E+09 |
| 23 | 4.979E+05 | 1.001E+10 | 1.040E+10 | 1.035E+10 |
| 24 | 3.688E+05 | 9.367E+09 | 9.430E+09 | 9.409E+09 |
| 25 | 2.972E+05 | 1.284E+10 | 1.319E+10 | 1.316E+10 |
| 26 | 1.832E+05 | 1.177E+10 | 1.185E+10 | 1.181E+10 |
| 27 | 1.111E+05 | 8.987E+09 | 9.102E+09 | 9.076E+09 |
| 28 | 6.738E+04 | 7.444E+09 | 7.496E+09 | 7.473E+09 |
| 29 | 4.087E+04 | 2.752E+09 | 2.796E+09 | 2.790E+09 |
| 30 | 3.183E+04 | 1.316E+09 | 1.432E+09 | 1.429E+09 |

**Table B.1 (continued)**

| Group number | Group upper energy limit | Neutron flux | | |
|---|---|---|---|---|
| | | BUGLE-93 | SAILOR-95 | BUGLE-96 |
| | eV | $cm^{-2}\ s^{-1}$ | $cm^{-2}\ s^{-1}$ | $cm^{-2}\ s^{-1}$ |
| 31 | 2.606E+04 | 2.557E+09 | 2.578E+09 | 2.571E+09 |
| 32 | 2.418E+04 | 1.539E+09 | 1.552E+09 | 1.546E+09 |
| 33 | 2.188E+04 | 3.961E+09 | 4.038E+09 | 4.027E+09 |
| 34 | 1.503E+04 | 7.440E+09 | 7.589E+09 | 7.550E+09 |
| 35 | 7.102E+03 | 8.556E+09 | 8.686E+09 | 8.663E+09 |
| 36 | 3.355E+03 | 7.928E+09 | 8.047E+09 | 8.024E+09 |
| 37 | 1.585E+03 | 1.302E+10 | 1.332E+10 | 1.328E+10 |
| 38 | 4.540E+02 | 7.223E+09 | 7.381E+09 | 7.362E+09 |
| 39 | 2.144E+02 | 7.900E+09 | 8.050E+09 | 8.031E+09 |
| 40 | 1.013E+02 | 1.037E+10 | 1.056E+10 | 1.053E+10 |
| 41 | 3.727E+01 | 1.265E+10 | 1.288E+10 | 1.284E+10 |
| 42 | 1.068E+01 | 7.259E+09 | 7.383E+09 | 7.365E+09 |
| 43 | 5.043E+00 | 9.579E+09 | 9.360E+09 | 9.384E+09 |
| 44 | 1.855E+00 | 7.103E+09 | 6.297E+09 | 6.357E+09 |
| 45 | 8.764E-01 | 6.081E+09 | 4.893E+09 | 4.933E+09 |
| 46 | 4.140E-01 | 1.268E+10 | 7.068E+09 | 7.074E+09 |
| 47 | 1.000E-01 | 2.709E+10 | 5.339E+09 | 9.820E+09 |
| | 1.000E-05* | | | |

* Low-energy boundary of the last group.

**TABLE B.2 Calculated multigroup neutron fluxes at the location of cavity dosimeters** (0° azimuth, core midplane, at the radius of 238.02 cm from core vertical axes)

| Group number | Group upper energy limit | Neutron flux BUGLE-93 | Neutron flux SAILOR-95 | Neutron flux BUGLE-96 |
|---|---|---|---|---|
| | eV | $cm^{-2}s^{-1}$ | $cm^{-2}s^{-1}$ | $cm^{-2}s^{-1}$ |
| 1 | 1.733E+07 | 1.385E+05 | 1.386E+05 | 1.386E+05 |
| 2 | 1.419E+07 | 3.917E+05 | 3.915E+05 | 3.918E+05 |
| 3 | 1.221E+07 | 1.544E+06 | 1.544E+06 | 1.545E+06 |
| 4 | 1.000E+07 | 2.828E+06 | 2.827E+06 | 2.827E+06 |
| 5 | 8.607E+06 | 4.247E+06 | 4.251E+06 | 4.248E+06 |
| 6 | 7.408E+06 | 8.486E+06 | 8.507E+06 | 8.487E+06 |
| 7 | 6.065E+06 | 1.185E+07 | 1.190E+07 | 1.185E+07 |
| 8 | 4.966E+06 | 2.262E+07 | 2.284E+07 | 2.265E+07 |
| 9 | 3.679E+06 | 1.910E+07 | 1.929E+07 | 1.918E+07 |
| 10 | 3.012E+06 | 1.572E+07 | 1.594E+07 | 1.585E+07 |
| 11 | 2.725E+06 | 1.992E+07 | 2.020E+07 | 2.012E+07 |
| 12 | 2.466E+06 | 1.051E+07 | 1.075E+07 | 1.071E+07 |
| 13 | 2.365E+06 | 3.397E+06 | 3.494E+06 | 3.480E+06 |
| 14 | 2.346E+06 | 1.736E+07 | 1.788E+07 | 1.782E+07 |
| 15 | 2.231E+06 | 4.876E+07 | 5.011E+07 | 4.996E+07 |
| 16 | 1.920E+06 | 7.343E+07 | 7.712E+07 | 7.683E+07 |
| 17 | 1.653E+06 | 1.291E+08 | 1.379E+08 | 1.373E+08 |
| 18 | 1.353E+06 | 3.391E+08 | 3.705E+08 | 3.694E+08 |
| 19 | 1.003E+06 | 3.610E+08 | 3.967E+08 | 3.952E+08 |
| 20 | 8.208E+05 | 1.607E+08 | 1.745E+08 | 1.740E+08 |
| 21 | 7.427E+05 | 8.500E+08 | 1.038E+09 | 1.034E+09 |
| 22 | 6.081E+05 | 8.319E+08 | 8.919E+08 | 8.884E+08 |
| 23 | 4.979E+05 | 8.257E+08 | 9.839E+08 | 9.820E+08 |
| 24 | 3.688E+05 | 1.350E+09 | 1.609E+09 | 1.604E+09 |
| 25 | 2.972E+05 | 1.530E+09 | 1.692E+09 | 1.694E+09 |
| 26 | 1.832E+05 | 1.726E+09 | 1.870E+09 | 1.862E+09 |
| 27 | 1.111E+05 | 1.120E+09 | 1.150E+09 | 1.147E+09 |
| 28 | 6.738E+04 | 8.178E+08 | 7.908E+08 | 7.871E+08 |
| 29 | 4.087E+04 | 2.591E+08 | 2.583E+08 | 2.574E+08 |
| 30 | 3.183E+04 | 1.546E+08 | 1.613E+08 | 1.607E+08 |

**Table B.2 (continued)**

| Group number | Group upper energy limit | Neutron flux | | |
|---|---|---|---|---|
| | | BUGLE-93 | SAILOR-95 | BUGLE-96 |
| | eV | $cm^{-2} s^{-1}$ | $cm^{-2} s^{-1}$ | $cm^{-2} s^{-1}$ |
| 31 | 2.606E+04 | 5.410E+08 | 5.322E+08 | 5.319E+08 |
| 32 | 2.418E+04 | 3.489E+08 | 3.299E+08 | 3.285E+08 |
| 33 | 2.188E+04 | 5.325E+08 | 5.175E+08 | 5.163E+08 |
| 34 | 1.503E+04 | 6.552E+08 | 6.657E+08 | 6.612E+08 |
| 35 | 7.102E+03 | 6.656E+08 | 6.775E+08 | 6.739E+08 |
| 36 | 3.355E+03 | 5.392E+08 | 5.508E+08 | 5.480E+08 |
| 37 | 1.585E+03 | 7.867E+08 | 8.201E+08 | 8.160E+08 |
| 38 | 4.540E+02 | 3.945E+08 | 4.130E+08 | 4.112E+08 |
| 39 | 2.144E+02 | 3.872E+08 | 4.057E+08 | 4.041E+08 |
| 40 | 1.013E+02 | 4.742E+08 | 4.975E+08 | 4.957E+08 |
| 41 | 3.727E+01 | 5.282E+08 | 5.547E+08 | 5.529E+08 |
| 42 | 1.068E+01 | 2.813E+08 | 2.955E+08 | 2.946E+08 |
| 43 | 5.043E+00 | 3.373E+08 | 3.392E+08 | 3.385E+08 |
| 44 | 1.855E+00 | 2.306E+08 | 2.133E+08 | 2.135E+08 |
| 45 | 8.764E-01 | 1.836E+08 | 1.692E+08 | 1.692E+08 |
| 46 | 4.140E-01 | 3.610E+08 | 2.124E+08 | 2.123E+08 |
| 47 | 1.000E-01 | 8.827E+08 | 4.383E+08 | 4.397E+08 |
| | 1.000E-05* | | | |

* Low-energy boundary of the last group.

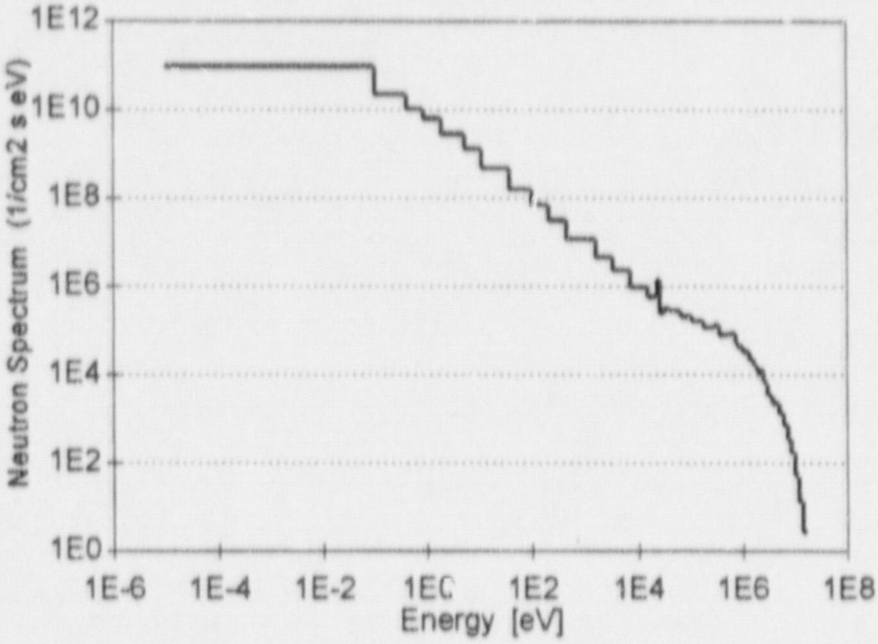


**Fig. B.1 Multigroup neutron spectrum, calculated with BUGLE-96 library, in the surveillance capsule** (20° azimuth, core midplane, at the radius of 191.15 cm from core vertical axis)

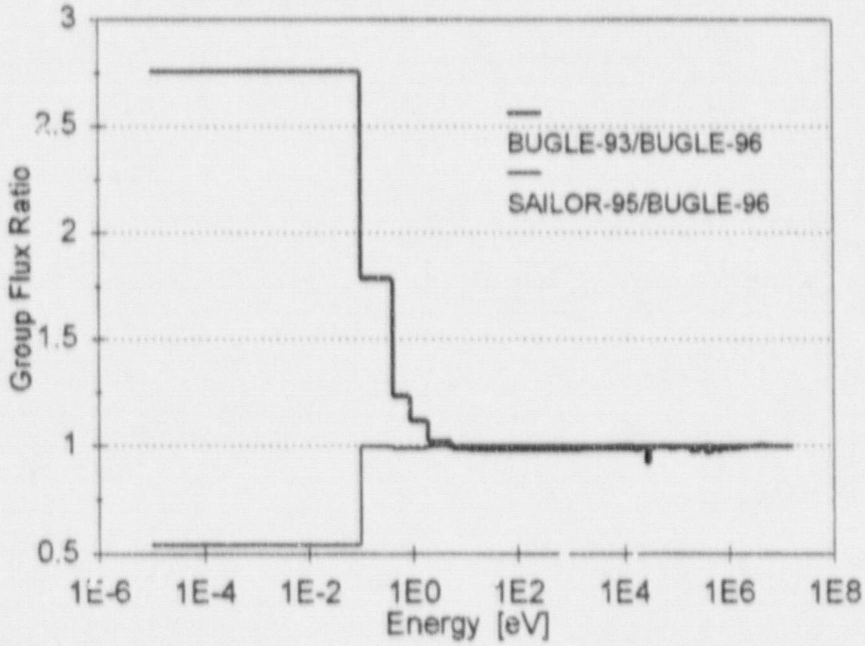


**Fig. B.2 Comparison of multigroup neutron spectra, calculated with different cross-section libraries, in the surveillance capsule** (20° azimuth, core midplane, at the radius of 191.15 cm from core vertical axis)

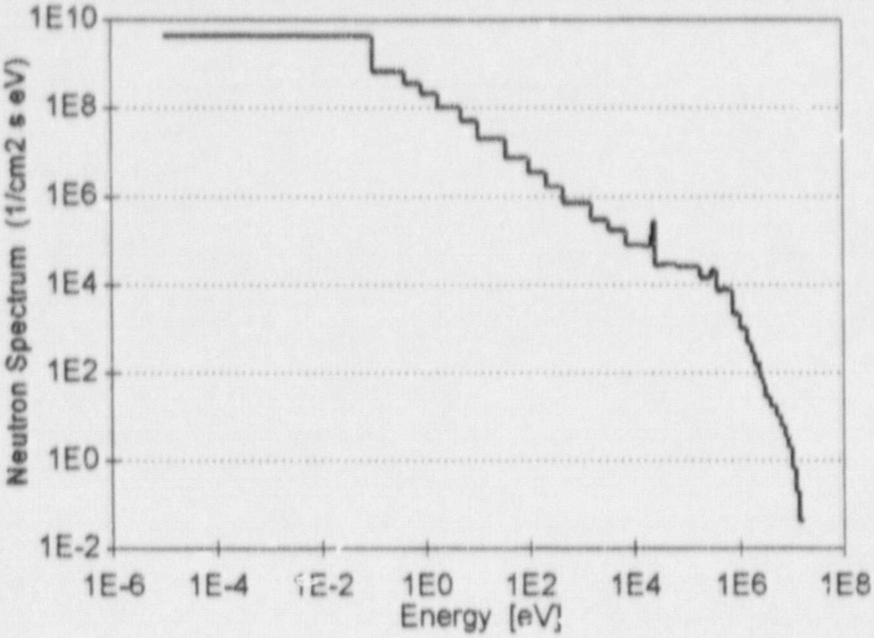


**Fig. B.3 Multigroup neutron spectrum, calculated with BUGLE-96 library, at the position of cavity dosimeters** (0° azimuth, core midplane, at the radius of 238.02 cm from core vertical axis)

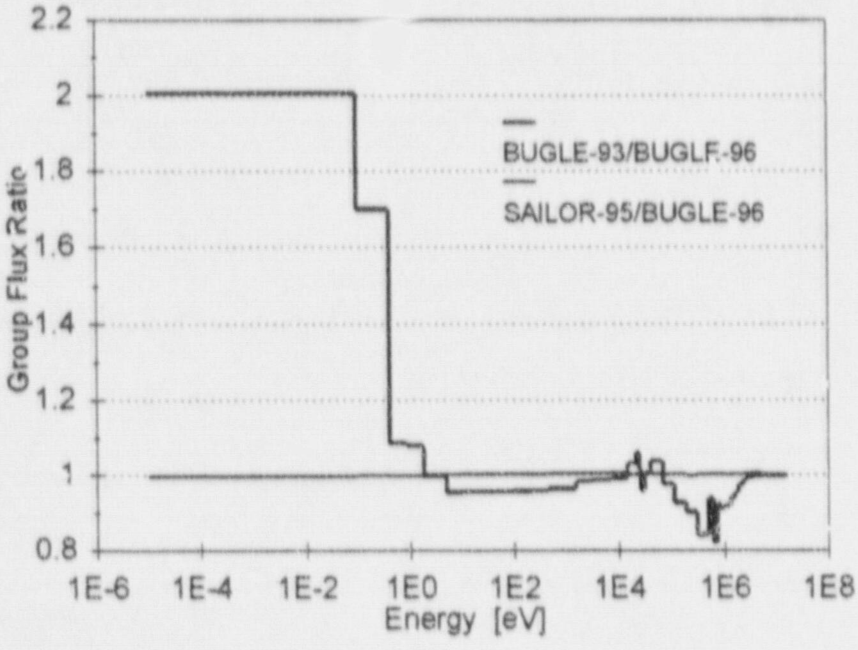


**Fig. B.4 Comparison of multigroup neutron spectra, calculated with different cross-section libraries, at the position of cavity dosimeters** (0° azimuth, core midplane, at the radius of 238.02 cm from core vertical axis)

NRC FORM 335
(2-89)
NRCM 1102,
3201, 3202

U.S. NUCLEAR REGULATORY COMMISSION

# BIBLIOGRAPHIC DATA SHEET

*(See instructions on the reverse)*

**1. REPORT NUMBER** (Assigned by NRC, Add Vol., Supp., Rev., and Addendum Numbers, if any.)

NUREG/CR-6453
ORNL/TM-13204

**2. TITLE AND SUBTITLE**

H. B. Robinson-2 Pressure Vessel Benchmark

**3. DATE REPORT PUBLISHED**

| MONTH | YEAR |
|---|---|
| February | 1998 |

**4. FIN OR GRANT NUMBER**

W6164

**5. AUTHOR(S)**

I. Remec, F. B. K. Kam

**6. TYPE OF REPORT**

**7. PERIOD COVERED** (Inclusive Dates)

**8. PERFORMING ORGANIZATION – NAME AND ADDRESS** (If NRC, provide Division, Office or Region, U.S. Nuclear Regulatory Commission, and mailing address; if contractor, provide name and mailing address.)

Oak Ridge National Laboratory
Oak Ridge, TN 37831-6363

**9. SPONSORING ORGANIZATION – NAME AND ADDRESS** (If NRC, type "Same as above"; if contractor, provide NRC Division, Office or Region, U.S. Nuclear Regulatory Commission, and mailing address.)

Division of Engineering Technology
Office of Nuclear Regulatory Research
U.S. Nuclear Regulatory Commission
Washington, D.C. 20555-0001

**10. SUPPLEMENTARY NOTES**

C. J. Fairbanks, NRC Project Manager

**11. ABSTRACT** (200 words or less)

The HBR-2 benchmark is specified and analyzed in this report. Analysis of the HBR-2 benchmark can be used as partial fulfillment of the requirements for the qualification of the methodology for calculating neutron fluence in pressure vessels, as required by the U.S. Nuclear Regulatory Commission's Regulatory Guide DG-1053, "Calculational and Dosimetry Methods for Determining Pressure Vessel Neutron Fluence."

Section 1 of this report provides all the dimensions, material compositions, and neutron source data necessary for the analysis. The measured quantities, to be compared with the calculated values, are the specific activities of the neutron dosimeters, on both sides of the pressure vessel: in the surveillance capsule attached to the thermal shield and in the reactor cavity.

Section 2 describes the analysis of the HBR-2 benchmark with the computer code DORT and three ENDF/B-VI based multigroup libraries. The average ratio of the calculated-to-measured specific activities (C/M) for the six dosimeters in the surveillance capsule was 0.90 ± 0.04 for all three libraries. The average C/Ms for the cavity dosimeters (without neptunium dosimeter) were 0.89 ± 0.10, 0.91 ± 0.10, and 0.90 ± 0.09 for the BUGLE-93, SAILOR-95, and BUGLE-96 libraries, respectively.

**12. KEY WORDS/DESCRIPTORS** (List words or phrases that will assist researchers in locating the report.)

Neutron dosimetry
Neutron transport calculations
Qualification of the calculational methodology
Reactor pressure vessel
ENDF/B-VI
Benchmark
HBR-2

**13. AVAILABILITY STATEMENT**

Unlimited

**14. SECURITY CLASSIFICATION**

(This Page)
Unclassified

(This Report)
Unclassified

**15. NUMBER OF PAGES**

**16. PRICE**

Printed on recycled paper

Federal Recycling Program

UNITED STATES
NUCLEAR REGULATORY COMMISSION
WASHINGTON, DC 20555-0001

OFFICIAL BUSINESS
PENALTY FOR PRIVATE USE, $300

FIRST CLASS MAIL
POSTAGE AND FEES PAID
USNRC
PERMIT NO. G-67

120555154486 1 1AN
US NRC-OIRM
TPS-PDR-NUREG
2WFN-6E7
WASHINGTON DC 20555